Experimental Neurology 350 (2022) 113969

Contents lists available at ScienceDirect

Experimental Neurology

journal homepage: www.elsevier.com/locate/yexnr

Research paper

Early derailment of firing properties in CA1 pyramidal cells of the ventral hippocampus in an Alzheimer's disease mouse model

Elena Spoleti [a,1], Paraskevi Krashia [b,c,1], Livia La Barbera [a,c], Annalisa Nobili [a,c], Carmen Alina Lupascu [d], Elisabetta Giacalone [d], Flavio Keller [b], Michele Migliore [d], Massimiliano Renzi [e,2,*], Marcello D'Amelio [b,c,2,**]

[a] Faculty of Sciences and Technologies for Humans and Environment, University Campus Bio-Medico, Rome 00128, Italy
[b] Faculty of Medicine and Surgery, University Campus Bio-Medico, Rome 00128, Italy
[c] Department of Experimental Neurosciences, IRCCS Santa Lucia Foundation, Rome 00143, Italy
[d] Institute of Biophysics, National Research Council, Palermo 90146, Italy
[e] Department of Physiology and Pharmacology, Sapienza University, Rome 00185, Italy

ARTICLE INFO

Keywords:
Alzheimer's disease
CA1
Ventral tegmental area
Dopamine
Tg2576
Excitability
Hippocampus
Pyramidal neuron
Computational modelling

ABSTRACT

Gradual decline in cognitive and non-cognitive functions are considered clinical hallmarks of Alzheimer's Disease (AD). Post-mortem autoptic analysis shows the presence of amyloid β deposits, neuroinflammation and severe brain atrophy. However, brain circuit alterations and cellular derailments, assessed in very early stages of AD, still remain elusive. The understanding of these early alterations is crucial to tackle defective mechanisms.

In a previous study we proved that the Tg2576 mouse model of AD displays functional deficits in the dorsal hippocampus and relevant behavioural AD-related alterations. We had shown that these deficits in Tg2576 mice correlate with the precocious degeneration of dopamine (DA) neurons in the Ventral Tegmental Area (VTA) and can be restored by L-DOPA treatment. Due to the distinct functionality and connectivity of dorsal *versus* ventral hippocampus, here we investigated neuronal excitability and synaptic functionality in the ventral CA1 hippocampal sub-region of Tg2576 mice. We found an age-dependent alteration of cell excitability and firing in pyramidal neurons starting at 3 months of age, that correlates with reduced levels in the ventral CA1 of tyrosine hydroxylase – the rate-limiting enzyme of DA synthesis. Additionally, at odds with the dorsal hippocampus, we found no alterations in basal glutamatergic transmission and long-term plasticity of ventral neurons in 8-month old Tg2576 mice compared to age-matched controls. Last, we used computational analysis to model the early derailments of firing properties observed and hypothesize that the neuronal alterations found could depend on dysfunctional sodium and potassium conductances, leading to anticipated depolarization-block of action potential firing. The present study depicts that impairment of cell excitability and homeostatic control of firing in ventral CA1 pyramidal neurons is a prodromal feature in Tg2576 AD mice.

1. Introduction

Alzheimer's disease (AD) is the most common form of dementia, characterized by progressive neurodegeneration causing cognitive decline associated with neuropsychiatric symptoms (Ballard et al., 2011; Blennow et al., 2006; Masters et al., 2015). For more than 25 years research in the field has linked the pathogenesis of AD to the so-called "amyloid hypothesis"; yet, the ability of new amyloid β (Aβ)-targeting drugs to provide a real clinical benefit to patients is still controversial, despite being successful in reducing the amyloid charge and other pathophysiological markers (Mintun et al., 2021; Rabinovici, 2021; Swanson et al., 2021; see also Canter et al., 2016; Chételat, 2013; Hardy and Selkoe, 2002; Herrup, 2015).

In the last years, even within variability in familial AD models and

* Corresponding author at: Department of Physiology and Pharmacology, Sapienza University, Rome 00185, Italy
** Corresponding author at: Faculty of Medicine and Surgery, University Campus Bio-Medico, Rome 00128, Italy.
E-mail addresses: massimiliano.renzi@uniroma1.it (M. Renzi), m.damelio@unicampus.it (M. D'Amelio).
[1] These authors contributed equally.
[2] These authors contributed equally.

https://doi.org/10.1016/j.expneurol.2021.113969
Received 27 September 2021; Received in revised form 6 December 2021; Accepted 27 December 2021
Available online 31 December 2021

experimental conditions, functional changes in the hippocampal network preceding the appearance of pathological aggregates were also well documented (Bateman et al., 2012; D'Amelio and Rossini, 2012; Mondadori et al., 2006; Palop and Mucke, 2016; Reiman et al., 2012). In this context, several lines of evidence have underlined the importance of dopamine (DA) in the progression of AD. In light of its importance for hippocampal-dependent memory (Bethus et al., 2010; Broussard et al., 2016; Lisman and Grace, 2005; McNamara et al., 2014; Rosen et al., 2015; Rossato et al., 2009; Yang et al., 2017), many early studies established a link between deficits in mesocorticolimbic DA signalling and early AD (Allard et al., 1990; Gibb et al., 1989; Joyce et al., 1997; Kemppainen et al., 2003; Koch et al., 2014; Kumar and Patel, 2007; Murray et al., 1995; Rinne et al., 1986a, 1986b; Storga et al., 1996). Notably, several dopaminergic drugs have been shown to exert positive effects in AD patients (Koch et al., 2011, 2014, 2020; Martorana and Koch, 2014; Monteverde et al., 1990) and enhancement of the dopaminergic drive has been shown to improve dysfunctional synaptic plasticity, cognitive impairment and memory in various animal models of the disease (Ambrée et al., 2009; Guzmán-Ramos et al., 2012; Hao et al., 2015; Himeno et al., 2011; Jürgensen et al., 2011; Pazini et al., 2013; Tsunekawa et al., 2008). These works support the notion that the mesocorticolimbic DA system undergoes profound changes since the very early phases of the disease.

In line with this notion, we have recently reported that dopaminergic, tyrosine hydroxylase (TH)-positive neurons in the Ventral Tegmental Area (VTA) of the transgenic mouse Tg2576 (a well characterized mouse model of AD over-expressing the human amyloid precursor protein carrying the Swedish mutation; Hsiao et al., 1996), undergo progressive degeneration starting between the 2nd and 3rd month of age (Nobili et al., 2017). By the 6th month, this selective neurodegeneration in Tg2576 mice leads to the detectable reduction of DA in brain areas innervated by the VTA, such as the nucleus accumbens (NAc) *shell* and dorsal hippocampus (Nobili et al., 2017). Notably, alterations mirroring the timeline of dopaminergic neuron loss have been reported in these animals at the behavioural, functional and cellular level. Thus, at 6 months of age Tg2576 mice show reduced reward conditioning (CPP task) correlating with low DA in the NAc *shell*, reduced excitability of dorsal pre-Subicular neurons and defective glutamatergic transmission into the NAc *core* (Cordella et al., 2018; Nobili et al., 2017). Likewise, the impaired memory performance (fear conditioning, novel object recognition and Morris Water Maze tests) in 3–6 months-old Tg2576 mice correlates with fewer dendritic spines and altered synaptic markers in dorsal hippocampal neurons, as well as with reduced LTP at CA3 – CA1 or dentate gyrus synapses (Corsetti et al., 2020; D'Amelio et al., 2011; Jacobsen et al., 2006; Nobili et al., 2017). The relevance of the dysfunctional dopaminergic system to these alterations is supported by different observations; firstly, memory and reward impairments well anticipate Aβ deposition (starting in these mice around the 11th month of age; Hsiao et al., 1996; Irizarry et al., 1997) and, instead, temporally correlate with loss of TH^+ VTA neurons. Also, and more importantly, these deficits are rescued by sub-chronic treatment with either the DA precursor L-DOPA or with selegiline, an inhibitor of monoamine oxidase B (Cordella et al., 2018; Nobili et al., 2017). In fact, both decreased release of DA in the dorsal hippocampus and relevant memory deficits in Tg2576 mice can be prevented by reducing the loss of TH^+ VTA neurons (La Barbera et al., 2021). Importantly, the involvement of the VTA in AD has been recently confirmed in Mild Cognitive Impairment (MCI) and AD patients, showing significant functional, structural and metabolic changes affecting the VTA and its cortical or sub-cortical projection areas, including the hippocampus (D'Amelio et al., 2018a, 2018b; De Marco and Venneri, 2018; Iaccarino et al., 2020; Sala et al., 2021; Serra et al., 2018, 2021; Venneri and De Marco, 2020).

Growing evidence prompt to re-consider the hippocampus as a *unicum*, with its dorsal and ventral areas distinct for innervation inputs, projection targets and role in behaviour (Kheirbek et al., 2013; Strange et al., 2014). Based on this reasoning, the dorsal hippocampus, which corresponds to the posterior hippocampus in primates, is generally believed to perform primarily cognitive functions and mediate several forms of memory (episodic memory, spatial learning). Instead, the ventral hippocampus (anterior in primates) relates mostly to stress responses and emotional behaviour (Fanselow and Dong, 2010; Kheirbek et al., 2013; Moser and Moser, 1998). This dual function of the hippocampus and its close functional relationship with the VTA suggest that deficits in the VTA-hippocampus loop in AD would affect not only cognitive functions and memory, but also non-cognitive functions as well (Serra et al., 2018, 2021).

Given this functional heterogeneity between dorsal and ventral hippocampus, and considering that only few studies have focussed on the role of the ventral hippocampus in AD (Maruszak and Thuret, 2014; Xu et al., 2021; Zarei et al., 2013), here we asked whether ventral hippocampal neurons could be affected in Tg2576 mice similarly to what observed in the dorsal region. To address this, we used slice patch-clamp and field recordings to investigate neuronal excitability, excitatory synaptic drive and synaptic plasticity in pyramidal neurons of the ventral CA1 from Tg2576 vs WT mice. We chose two age-windows, that is 2-to-3 and 6-to-8 months of age, thus respectively at the onset and well into the loss of dopaminergic neurons in the VTA of this AD model. We have found that already at 3 months of age ventral CA1 neurons of Tg2576 mice show altered excitability and firing profile without alterations in glutamatergic synaptic transmission, plasticity and dendrite branching. We then quantified both TH levels and Aβ load as well as microglia-related neuroinflammation to gain insights on possible causes contributing to such alterations. Lastly, we used computational modelling of our patch-clamp data to propose possible mechanisms underlying the electrophysiological impairments observed in neurons.

2. Materials and methods

2.1. Animals

Heterozygous Tg2576 mice and wild-type (WT) littermates (both males and females) were used at 2.5–3 or 6–8 months of age (range: P78–97, insofar indicated as 3 months-old; and P181–240, insofar indicated as 8 months-old, respectively). All animal experiments complied with the ARRIVE guidelines and were carried out in accordance with the ethical guidelines of the European Council Directive (2010/63/EU); experimental approval was obtained from the Italian Ministry of Health (protocol #926/2018PR).

2.2. Acute brain slice preparation

Mice were anaesthetized with halothane and perfused transcardially with cold (0.5–4 °C), oxygenated (95% O_2, 5% CO_2) 'slicing' solution, containing (mM): NMDG 92, KCl 2.5, NaH_2PO_4 1.2, $NaHCO_3$ 30, HEPES 20, Glucose 25, Na-ascorbate 5, Thiourea 2, Na-pyruvate 3, $MgSO_4$ 10, $CaCl_2$ 0.5 (pH 7.4 with HCl, ~ 295–310 mOsm; Ting et al., 2018). After the mouse liver turned from deep red to pale yellow, mice were decapitated, and the brains rapidly removed and dissected. Transverse slices containing the ventral hippocampus (350 μm-thick; within 1.25–2.30 mm from the ventral surface of the brain) were cut using a vibratome (VT1200S, Leica) in chilled, oxygenated slicing solution. After cutting, brain slices were transferred into a holding chamber containing the same solution and incubated at 34 °C for 25–35 min (depending on mouse age) while slowly increasing NaCl to a final concentration of approx. 90 mM (see Ting et al., 2018). Finally, slices were transferred into a recovery chamber with 'maintenance' solution, containing (mM): NaCl 92, KCl 2.5, NaH_2PO_4 1.2, $NaHCO_3$ 30, HEPES 20, Glucose 25, Na-ascorbate 5, Thiourea 2, Na-pyruvate 3, $MgSO_4$ 2, $CaCl_2$ 2 (pH 7.3–7.4 with NaOH, ~ 300–310 mOsm) where they were kept at room temperature until use.

2.3. Electrophysiology

Patch-clamp recording from CA1 pyramidal neurons: For patch-clamp recordings slices were transferred to a submerged chamber and perfused with oxygenated artificial Cerebro-Spinal Fluid (aCSF; 3–4 ml/min) containing (in mM): 125 NaCl, 3 KCl, 26 $NaHCO_3$, 1.25 $NaHPO_4$, 10 Glucose, 1 $MgCl_2$, 2 $CaCl_2$ (pH ~ 7.3). CA1-preSubicular neurons (here referred to as 'CA1') were visualized using the IR-DIC optics of an upright Leica DMLSF microscope and current- or voltage-clamp recordings were obtained using a MultiClamp 700B amplifier and the pClamp9 suite (Molecular Devices). All recordings were performed at room temperature (~ 24 °C).

For current-clamp and recording of spontaneous Excitatory Post-Synaptic Currents (sEPSCs), the 'intracellular' pipette solution contained (in mM): 110 K-gluconate, 12 KCl, 10 HEPES, 10 Na_2-phosphocreatine, 4 Mg_2-ATP, 0.3 Na_2-GTP, 0.1 EGTA-K (pH 7.3 with KOH; 295 mOsm). For biocytin-filling we added freshly weighted biocytin (0.2–0.4%; Tocris) to the intracellular solution. Patch-pipettes were pulled (PC-10, Narishige) from thick-walled borosilicate glass (1.5 mm outer diameter and 0.86 mm inner diameter; GC150F-7.5; Harvard Apparatus), coated with Sylgard resin (Dow-Corning 184) and fire-polished (MF-830, Narishige) to a tip resistance of 3–8 MΩ. To improve whole-cell voltage-clamp, series resistance (R_s) was compensated (range 30–70%; average value after compensation 12.6 ± 0.9 MΩ, $n = 49$).

In current-clamp experiments, the intrinsic properties of pyramidal CA1 neurons were studied within the first 3 min after patch rupture; we injected families of current steps (I_{inj}) ranging in amplitude from – 0.2 to 0.6 nA (50 pA increments; 1 s duration) while holding the membrane potential at approximately – 80 mV (− 78 ± 0.3 mV, 66 neurons) by constant current injection. No drugs were added to the aCSF. In voltage-clamp experiments, sEPSCs were recorded holding the membrane potential at − 70 mV; estimated reversal potential for GABAergic synaptic currents was E_{rev}^{Cl} – 63 mV, thus no blockers were necessary to isolate glutamatergic currents.

Current-clamp recordings were filtered online at 10 kHz and sampled at 50 kHz; synaptic currents were filtered at 4 kHz and digitized at 20 kHz (amplifier in-built 8-pole low-pass Bessel filter and Molecular Devices Digidata 1322A, respectively).

Field Recordings: For field recording experiments, 6–8 months-old mice were anaesthetized with halothane and perfused transcardially with a cold (0.5–4 °C), oxygenated (95% O_2, 5% CO_2) 'sucrose-slicing' aCSF solution, containing, in mM: 3 KCl, 1.25 NaH_2PO_4, 26 $NaHCO_3$, 10 $MgSO_4$, 0.5 $CaCl_2$, 25 glucose, 185 sucrose; ~300 mOsm, pH 7.4.

After brain dissection, 350 μm-thick horizontal slices were prepared in sucrose-slicing aCSF; recovery from slicing was performed in normal aCSF at 30 °C (40 min) and then at RT. For recording, slices were transferred into a submerged chamber of an upright microscope (Axioskop 2-FS; Zeiss, Germany) and perfused with oxygenated normal aCSF (3–4 ml/min; 30 °C) containing, in mM: 124 NaCl, 3 KCl, 1.25 NaH_2PO_4, 26 $NaHCO_3$, 1 $MgSO_4$, 2 $CaCl_2$, 10 Glucose (pH 7.4 with NaOH; ~300 mOsm).

Field Excitatory Post-Synaptic Potentials (fEPSPs) were recorded as previously described (Nobili et al., 2018). Briefly, to elicit standard field responses in the ventral hippocampus, the Schaffer collateral pathway was stimulated (pulse duration 100 μs; one pulse every 30 s) with an aCSF-filled borosilicate glass electrode placed in the striatum radiatum. The recording electrode (a borosilicate glass electrode filled with aCSF) was positioned in the stratum radiatum of the CA1 hippocampal region, 200–300 μm from the stimulating electrode. Input-output curves were obtained by measuring the slope of fEPSPs induced by stimulating the afferent pathway with incremental current steps (10 μA increments). In LTP experiments, if the fEPSP slope recorded appeared stable for at least 20 min the slice was challenged with two consecutive trains of stimuli (each 1–sec long and 100 Hz; 20 s apart) to induce synaptic plasticity; the field response was then recorded for at least 1 h. The degree of LTP was estimated at 55–60 min after the conditioning train as the mean fEPSP slope normalised to the mean baseline slope. Field responses were acquired using a MultiClamp 700B amplifier and digitized using a Digidata 1322A (20 kHz sampling). For both acquisition and analysis of field responses we used pClamp9.2.

2.4. Data analysis

The neuron resting potential (RP) was estimated using the amplifier inbuilt voltmeter immediately after gaining cell access. Analysis of current-clamp and voltage-clamp recordings was performed using Igor. Pro 6.32A (WaveMetrics Inc.) with NeuroMatic 2.8 (Rothman and Silver, 2018). The membrane time constant (τ_m) was calculated in voltage-clamp as weighted tau of the double-exponential fit of the decay of the whole-cell current elicited in response to a – 5 mV seal voltage-step (V_{step}; − 70 mV holding potential). The membrane capacitance (C_m) was then calculated as τ_m / R_s, where $R_s = V_{step} / I_c$ (peak of the capacitive current).

The 'sag' of the membrane potential response to current injection was calculated as the percentage difference between the minimum amplitude of the initial response relative to the minimum amplitude of the steady-state response, both calculated from a 5-ms averaging window with respect to the average baseline (200 ms). Sag values were obtained for the first three hyperpolarizing current steps (− 0.20, − 0.15 and – 0.10 nA) and averaged (Suter et al., 2013).

The input resistance (R_{in}) was estimated as the slope of a linear least-squares fit to the relationship between the amplitude of five sub-threshold steps of injected currents (range: – 0.20-0 nA; 1 s duration; cells held at − 80 mV) and the steady-state voltage response of the cell.

The rheobase, the amplitude of the injected current necessary to induce the first action potential (AP), was estimated graphically (Clampfit) from the voltage response to a series of 5 pA-incremented consecutive steps of I_{inj} (50 ms duration; range: 0 ÷ 0.4 nA). To quantify the AP threshold, phase-plane plots of dV_m/dt versus V_m ('phase plots') were built for the first AP induced during the rheobase protocol. Spike threshold was estimated as the membrane potential value at which dV_m/dt increased suddenly and developed with a monotonic rise (Bean, 2007; Trombin et al., 2011).

To study cell excitability, curves describing the relationship between the frequency of induced APs and the injected current were compared and their maximal gain was quantified for each cell as the slope of the linear fit to the curve. Detection of APs was performed in NeuroMatic using a threshold (+ 5 mV) crossing method. Due to the presence of depolarization-block, we estimated the maximal gain of the f – I curve normally within its first supra-threshold responses. The peak of the medium after-hyperpolarization (mAHP) was quantified as the minimum value reached by the membrane potential within a time window of 200 ms immediately after the end of the stimulation protocol (average of 5 ms after baseline subtraction). To quantify the firing adaptation, the Spike Frequency Adaptation (SFA) factor was calculated from the average of the last 2 inter-spike intervals (ISIs) divided by the average of the first 2 ISIs when the neuron fired at ~14 Hz (13.8 ± 0.3 Hz, 53 cells, range 9–19 Hz; Suter et al., 2013).

For analysis of sEPSCs, detection of synaptic currents was performed non-automatically using an amplitude threshold crossing approach in Clampfit 10.7 (Molecular Devices; dwell times shorter than 1 ms were skipped). Three different analysis windows (at least 30-s long) per cell were scanned and each synaptic event was fitted using a custom-made triple-exponential function (eq. 1; NeuroMatic),

$$f(x) = \left(1 - exp\left(-\frac{x - X0}{TR}\right)\right)^{N} * \left(A1 * exp\left(-\frac{x - X0}{TD1}\right) + A2 * exp\left(-\frac{x - X0}{TD2}\right)\right) \quad (1)$$

where: TR was the current 10–90% rise-time; and TD_n, A_n were the n^{th} component of decay and relevant fractional amplitude, respectively.

To maximize the signal-to-noise ratio, peak amplitude (I_{peak}) and kinetic analysis were performed from current fits (NeuroMatic). Current decay was estimated from the current fit using a double-exponential function (eq. 2); the weighted time constant of the decay (T_w) was calculated as the sum of the fast and slow time constants weighted by their fractional amplitudes (A1, A2).

$$f(x) = y0 + A1e^{\frac{-(x-x0)}{t1}} + A2e^{\frac{-(x-x0)}{t2}} \quad (2)$$

Average values of 10–90% rise-time, I_{peak} and T_w were calculated for each cell after checking their time stability using the NeuroMatic built-in function derived from a Spearman Rank-Order macro; segments that lacked time stability were excluded.

2.5. Immunofluorescence

Mice were anaesthetized with Rompun (20 mg ml-1, 0.5 ml kg-1, i.p., Bayer) and Zoletil (100 mg ml-1, 0.5 ml kg-1, Virbac) and perfused transcardially with 50 ml saline followed by 50 ml of 4% paraformaldehyde in Phosphate Buffer (PB; 0.1 M, pH 7.4). The brains were removed and post-fixed in paraformaldehyde at 4 °C and then immersed in 30% sucrose solution at 4 °C until sinking. Brains were cut into 30 μm-thick horizontal sections using a cryostat and the slices were collected in PB.

For TH immunofluorescent labelling, selected sections were incubated in citrate buffer (10 mM Sodium citrate, pH 6.0 containing 0.05% Triton X-100; 20 min, 75 °C), rinsed in PB, immersed in blocking solution (5% donkey serum, 0.2% Triton X-100 in PB) for 1 h, and incubated with primary antibody in blocking solution (overnight at 4 °C). After three washes in PB, sections were incubated with a secondary antibody in blocking solution. For Iba1 and Aβ immunofluorescent labelling, sections were incubated overnight with primary antibodies in PB containing 0.3% Triton X-100 and then incubated for 2 h at room temperature with secondary antibodies.

For 3D reconstruction of TH^+ fibers, Iba1 cells and biocytin-filled neurons, images were taken as *Z*-stacks and these were then processed by maximum intensity projection.

All samples were acquired with the same laser settings. For quantification of TH and Aβ expression levels, images were collected from at least 4–5 slices processed simultaneously from the ventral hippocampus and exported for analysis with ImageJ software (http://imagej.nih.gov/ij/) as mean fluorescence intensity (F) over a defined area (A).

For analysis of biocytin-filled neurons, slices bearing neurons loaded with biocytin were fixed by immersion in 4% paraformaldehyde in PB overnight (4 °C). Then, slices were washed three times in PB and incubated with 555-conjugated Streptavidin in PB containing 0.3% Triton X-100 (4 °C overnight). Finally, neurons were analysed with Neurolucida 7.5 software (MicroBright-Field; see below).

Primary antibodies: TH (1:1000, ABCAM; AB112; RRID: AB_297840); Iba1 (1:800; Wako #019–19741; RRID: AB_839504); hAPP695 (6E10; 1:500, BioLegend; #803001; RRID: AB_2564653); NeuroTrace-405 (1:200, Thermo Fisher Scientific; #N21479).

Secondary antibodies: Alexa Fluor 488 donkey anti-rabbit IgG (1:200; Thermo Fisher Scientific; # A32790; RRID: AB_2762833); Alexa Fluor 488 donkey anti-mouse IgG (1:200; Thermo Fisher Scientific; #R37114; RRID: AB_2556542); Streptavidin, Alexa Fluor 555-Conjugate (1:750; Invitrogen #S32355; RRID:AB_2571525).

Sections for immunofluorescence were counterstained with DAPI (1:1000; 5 min) or NeuroTrace 640/660 (1:200, Thermo Fisher Scientific, # N21483), coverslipped with Aqueous Mounting Media (Sigma-Aldrich) and examined under a confocal laser-scanning microscope (LSM700, Zeiss). The immunofluorescence labelling specificity was confirmed by using normal serum instead of primary antibodies (negative controls).

2.6. Sholl analysis

$Iba1^+$ cells (microglia) and biocytin-filled pyramidal neurons in the ventral hippocampus were analysed by Sholl analysis (Krashia et al., 2019a). Cells were visualized with an optical microscope (DMLB; Leica) equipped with a motorized stage and a camera connected to Neurolucida 7.5 software (MicroBright-Field) that allowed for quantitative 3D analysis of the entire cell compartment. Only cells that showed intact processes unobscured by background labelling or other cells were included in the analysis. We evaluated the cell body area and perimeter, number of intersections and total length of processes. To account for changes of cell complexity in relation to the distance from the soma, concentric circles originating from the soma (radii) were spaced 10 μm apart and the number of branch points, branch endings, cell processes intersecting the radii and cell process length were measured as a function of the distance from the cell soma. For $Iba1^+$ cells, fifteen cells per animal were selected randomly for analysis, all data were subsequently averaged for each mouse. For biocytin-filled pyramidal neurons, all cells were analysed for intersections of the apical dendrites.

2.7. Quantification of TH^+ fibre density

The quantification of TH^+ fibre numbers in the ventral hippocampus images was performed from at least 4 slices processed simultaneously and exported for analysis with ImageJ software (http://imagej.nih.gov/ij/) with a modified protocol (Sathyanesan et al., 2012). Images were converted in 8-bit and the background was removed using the tool 'region of interest Background subtraction'. The line scan profile analysis was performed with Image J "line tool". For each section, four horizontal lines (300 pixels) were drawn randomly in the CA1 and pixel intensity along the line was plotted using the "Plot Profile" tool. The total number of peaks per 300 pixels (plotted as TH^+ fibre density) deriving from the intensity matrices were counted manually. The data obtained from each animal were averaged and the data from 3 mice per genotype were used for the statistical analysis.

2.8. Computational modelling

All simulations were carried out using the NEURON simulator (v8.0.0; (Hines and Carnevale, 1997). Model and simulation files will be available in the ModelDB section of the Senselab database (https://senselab.med.yale.edu/modeldb/, acc.n. 267066).

For all simulations, we used a 3D reconstruction of a mouse hippocampal CA1 ventral pyramidal neuron (morphology NMO_114635, Ordemann et al., 2019), downloaded from Neuromopho.org (Ascoli, 2006). A 60 μm-long synthetic axon with a tapered diameter was added to the morphology. The electrophysiological traces from a few representative neurons for each strain and age were used as reference to implement a set of biophysically detailed neuron models. In particular, we chose recordings from: six neurons of 3 months-old WT mice; seven neurons of 3 months-old Tg2576 mice; five neurons of 8 months-old WT

Table 1
Sub-threshold and intrinsic properties of WT and Tg2576 (Tg) mice along development.

	τ_{memb} (ms)	R_{in} (MOhm)	C_m (pF)	Sag %	I_h (pA)
WT 3 m	1.7 ± 0.2 (12)	85 ± 8 (19)	93 ± 12 (12)	11 ± 2 (19)	−199 ± 32 (18)
Tg 3 m	1.4 ± 0.1 (17)	110 ± 11 (17)	72 ± 8 (17)	19 ± 1 (17) ***	−218 ± 31 (10)
WT 8 m	1.6 ± 0.2 (11)	104 ± 8 (13)	71 ± 14 (11)	13 ± 1 (13)	−170 ± 35 (9)
Tg 8 m	1.5 ± 0.2 (6)	115 ± 9 (13)	65 ± 9 (6)	16 ± 2 (13)	−209 ± 38 (5)

The table summarizes average ± s.e.m. values for membrane time constant (τ_{memb}), input resistance (R_{in}), capacitance (C_m), sag % and amplitude of I_h current. Data were compared across genotypes at 3 or 8 months of age. In brackets, number of cells analysed. All n.s. except for sag % in 3 months-old WT vs Tg mice: *** $p = 0.0003$ (all unpaired *t*-test with Welch's correction, except for 8-m I_h data: Mann Whitney test).

mice; and six neurons of 8 months-old Tg2576 mice.

Passive properties were manually tuned to match the observed input resistance and rheobase for each modelled neuron. The specific membrane capacitance was fixed at 1 μF/cm^2 and the temperature at 25 °C.

Active properties included: a transient Na^+ conductance; five types of K^+ currents (Delayed Rectifier, K_{DR}; A-type, K_V7; one type of slow Calcium-dependent current, K_{Ca}; and a voltage and Ca^{2+} dependent current); a non-specific I_h current; N-, T- and L-type Ca^{2+} current; and a simple Ca^{2+}-extrusion mechanism with a 100 ms time constant. The A-type K^+ and the I_h conductance were linearly increasing with distance from the soma. Channel kinetics and distribution were from a previously published model for CA1 pyramidal neurons (Migliore et al., 2018). The kinetic parameters of Na^+, delayed rectifier K^+ and K_V7-type K^+ channels were modified to fit the specific experimental findings of this paper (see the NEURON mod files in ModelDB for full details). To reproduce the depolarization block, we found that it was necessary to shift the Na^+ activation kinetic by +5 mV in the axon and by +10 mV in both soma and dendrites (Bianchi et al., 2012). The peak conductance of each channel type was manually tuned to fit, for each modelled neuron, the number of action potentials elicited experimentally as a function of the input current. To do this, we used a procedure aimed at identifying the minimal changes required to reproduce the experimental findings for each neuron population. The optimized values were compared using a Mann-Whitney Rank Sum Test; only parameters found to be statistically different ($p < 0.05$) were plotted.

2.9. Statistical analysis

Statistical tests were performed using Prism (GraphPad Software). Unless stated otherwise, differences between groups were examined using the appropriate paired or unpaired Student's *t*-test. When data were not normally distributed (Shapiro–Wilk test), we used a Mann–Whitney *U* test. *f* – *I* curves were examined using two-way repeated measures ANOVA (with genotype and injected current as independent factors); post-hoc comparisons were assessed with Bonferroni's or Tukey's tests. Differences were considered significant at $p < 0.05$ (*$p < 0.05$; ** $p < 0.01$; *** $p < 0.001$). All values are expressed as means ± s.e.m.

Neurons with max AP frequency ≤ 5 Hz or with resting potential more positive than – 50 mV were arbitrarily excluded from current-clamp analysis (9 excluded out of 71 cells). Neurons with outlying average frequency of synaptic events were arbitrarily excluded from voltage-clamp analysis (3 excluded from 47 cells). No correlation was evident between either genotype or age and exclusion condition (data not shown).

3. Results

3.1. Altered excitability of CA1 pyramidal neurons in the ventral hippocampus of Tg2576 mice

To investigate potential alterations in pyramidal neurons of the ventral CA1 in Tg2576 mice, we compared neurons from WT and Tg2576 mice of either 3 or 8 months of age, corresponding respectively to *early* and *overt* synaptic defects in the dorsal hippocampus of Tg2576 mice (Cordella et al., 2018; D'Amelio et al., 2011; Jacobsen et al., 2006; Nobili et al., 2017; Suppl. Fig. 1). At these time points, ventral CA1 neurons showed physiologically polarised resting potentials, independently of genotype (3 months-old mice: WT – 66 ± 1 mV, Tg2576 – 66 ± 1 mV; 19 and 17 cells from 5 mice; $p = 0.9686$; 8 months-old mice: WT – 68 ± 3 mV, Tg2576 – 65 ± 1 mV; both 13 cells from 3 mice; $p = 0.3205$). To assess membrane sub- and supra-threshold intrinsic properties in these cells, we presented neurons with families of current steps. Whilst the sub-threshold properties investigated appeared substantially unaltered across ages (Table 1), the rheobase was significantly different, with WT neurons undergoing an increase of their apparent excitability along development which lacked in Tg2576 animals (rheobase in 3 vs 8 months-old mice: WT, 283 ± 19 pA and 189 ± 14 pA, $p = 0.0005$; Tg2576, 208 ± 20 pA and 247 ± 17 pA, $p = 0.1508$; Fig. 1A). Thus, whilst rheobase was decreasing with age in WT mice, it stayed unaltered in Tg2576 animals. Consequently, when comparing ventral CA1 neurons from mice of the same age across strains, we found that the rheobase of Tg2576 pyramidal cells was significantly smaller in younger animals ($p = 0.0109$) and larger in older ones compared to WTs ($p = 0.0160$; Fig. 1A). This reflected into the relevant average *f* – I curves showing that ventral CA1 neurons of 8 months-old Tg2576 mice fired significantly less APs compared to WT neurons (3-months: $p = 0.5150$, $F_{1,32} = 0.4336$; 8-months: $p = 0.0433$, $F_{1,22} = 4.601$; Fig. 1B, analysis window in grey).

To start dissecting the ionic bases of the altered excitability found in Tg2576 animals, we analysed phase plots obtained from the first AP fired in response to the rheobase protocol. We found that the membrane voltage at which APs were fired ($V_{threshold}$, V_{thre}) was more depolarised in 8 months-old Tg2576 mice compared to WTs; instead, no differences emerged in younger animals (3-months: WT – 49 ± 1 mV and Tg2576 – 46 ± 1 mV, $p = 0.2537$; 8-months: WT – 53 ± 2 mV and Tg2576 – 45.7 ± 0.6 mV, $p = 0.0043$; Fig. 1C). Once over-threshold, WT and Tg2576 pyramidal neurons of both ages showed analogous firing properties, bearing same maximal slope ("gain") of the *f* – *I* curves, same maximal AP frequency and same spike accommodation (at the frequency range 10–20 Hz; Fig. 1D).

Together, these results show that cell excitability (rheobase and V_{thre}) and evoked firing (*f* – *I* curves) are altered in ventral CA1 neurons at early and later phases of disease onset in Tg2576 mice.

Our findings on the V_{thre} of APs in 8 months-old Tg2576 neurons are in line with the analysis of evoked excitability and provide insights into the mechanisms underlying the reduced input-output relationship observed in older Tg2576 mice, similarly to what we observed previously in pyramidal cells of the dorsal hippocampus (Cordella et al., 2018). On the other hand, differently from rheobase, the AP threshold of WT CA1 neurons showed no change along development. Rheobase is obviously affected not only by the V-gated Na^+ channel activation threshold, but also by the intrinsic, sub-threshold properties contributing to the readiness of the membrane to fire an AP. Indeed, when qualitatively considering at once R_{in} and C_m (Table 1), rheobase (Fig. 1A) and overall shape of the *f* – *I* curves (Fig. 1B) for each strain along development, we noticed that only WTs showed degrees of modification of these parameters with age, whilst Tg2576 ventral CA1 neurons had features typical of older mice already at three months of age, an intriguing point that we decided to investigate in more detail.

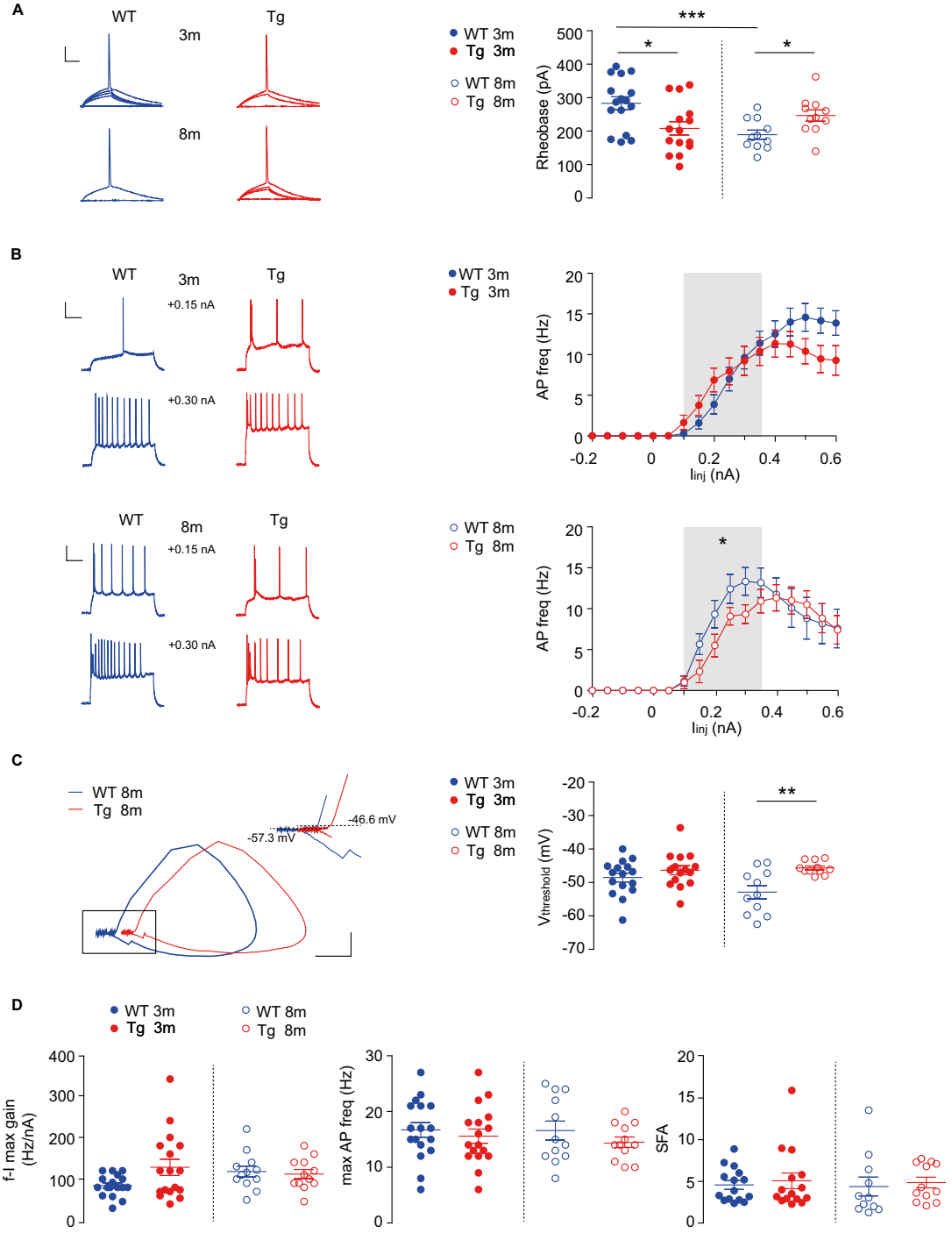

Fig. 1. Pyramidal neurons of the ventral CA1 from Tg2576 (Tg) mice show altered excitability. A, left: typical rheobase for WT and Tg CA1 neurons from 3- and 8-months old mice; cell response to selected current steps is depicted until the first AP (for stimulation protocol see Methods). Right: pooled data. Rheobase of WT and Tg CA1 neurons were significantly different both at 3 (* $p = 0.0109$; 16 WT and 15 Tg cells from 5 mice each) and at 8 months of age (* $p = 0.0160$; 11 cells from 3 mice each). Bars: 25 mV, 25 ms. Note that only in WTs the rheobase decreased along aging (WT *** $p = 0.0005$; Tg $p = 0.1508$). All unpaired *t*-test with Welch's correction. B, *f – I* relationships. Left, typical firing in response to depolarising current injections (bars: 25 mV, 250 ms). Right, full relationships for WT and Tg CA1 neurons at 3 and 8 months of age: Tg neurons showed reduced excitability at 8 months (* $p = 0.0433$), but not at 3 months ($p = 0.5150$; both 2-way RM ANOVA). The grey area indicates the stimulation range analysed (+ 0.1 ~ + 0.35 nA, chosen considering the presence of depolarization-block analysed separately in Fig. 2). For both WT and Tg: at 3 months, 17 cells from 5 mice; at 8 months, 12 cells from 3 mice. C, Phase plot analysis. Left, typical AP phase plots for CA1 neurons from 8 months-old WT or Tg mice (bars: 50 mV; 20 mV/ms) and relevant V_{thre} values (inset). Phase plots are depicted x-shifted for clarity. Right, pooled data. No difference was found across strains at 3 months of age ($p = 0.2537$; 16 WT and 15 Tg cells), but V_{thre} was significantly higher in Tg mice at 8 months (** $p = 0.0043$; 11 cells each strain). No difference was found along development for each strain: WT, 3 vs 8 months, $p = 0.0816$; Tg, 3 vs 8 months, $p = 0.6436$. All unpaired *t*-test with Welch's correction. D, Supra-threshold properties of analysed cells from WT and Tg mice. Pooled data depicting *f – I* max gain (left panel), maximal AP frequency (middle panel) and firing accommodation (SFA, estimated at the firing frequency of ~10÷20 Hz; right panel). All *p* values were within the range 0.21– 0.94 (SFA and max gain at 3 months: Mann Whitney test; all others: unpaired *t*-test with Welch's correction).

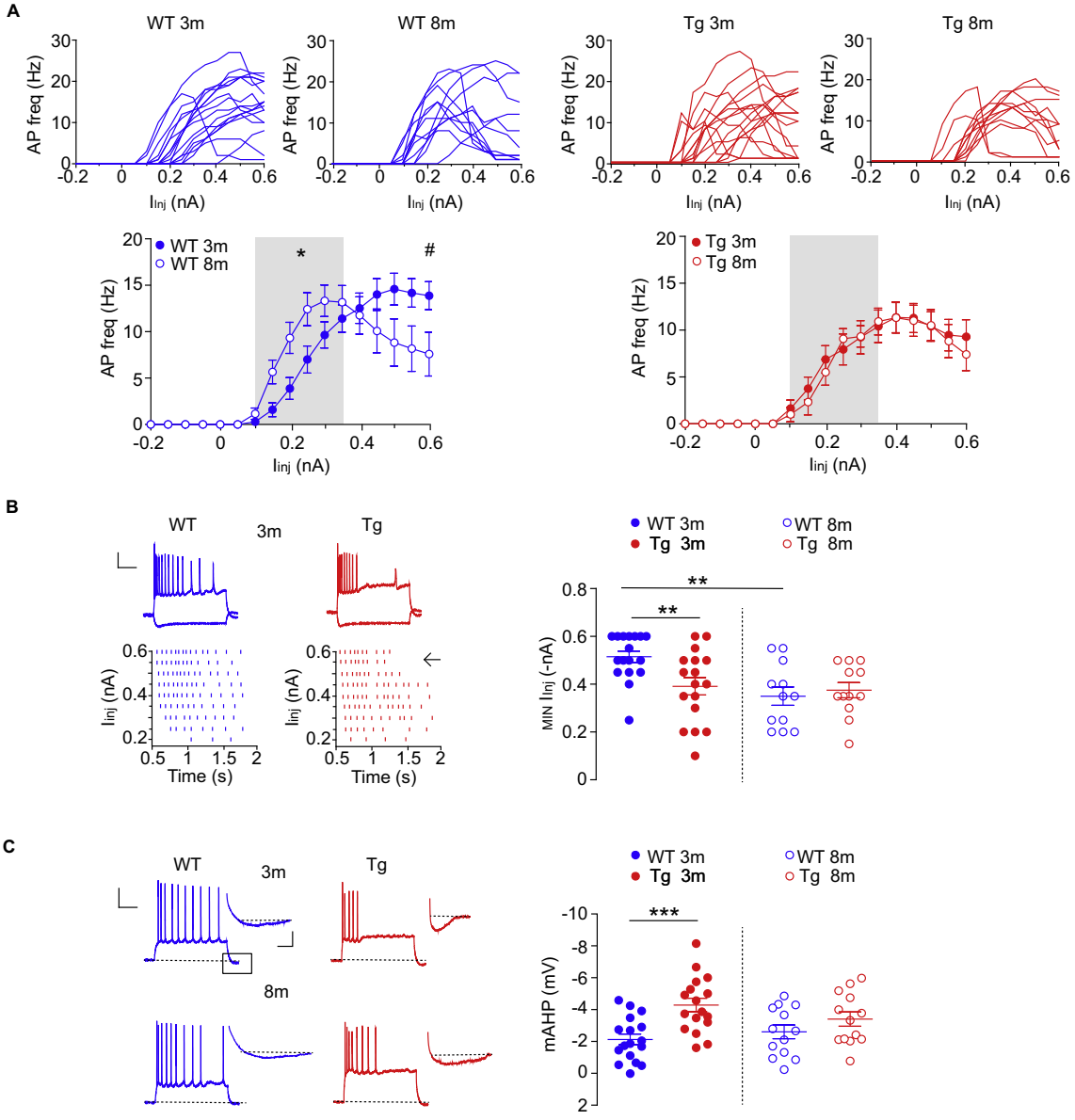

Fig. 2. Altered firing of ventral CA1 pyramidal neurons from Tg mice appears early during development. A, *f* – I relationships for WT and Tg mice at 3 and 8 months of age. Upper, all *f* – I curves analysed. Lower, pooled data. Note that neurons from younger and older WTs had different evoked firing, whilst Tg neurons showed almost identical input-output responses at different ages. The grey area indicates the stimulation range considered for 2-way RM ANOVA analysis (I_{inj} range: + 0.1 ~ + 0.35 nA; WT, * $p = 0.0304$; Tg, $p = 0.8473$; same cells/mice of Fig. 1). Also note that the reduction of firing rate in WTs was significant at I_{inj} + 0.6 nA (# $p = 0.0364$, unpaired t-test with Welch's correction; 17 WT and 12 Tg cells). B, Depolarization-block analysis. Left, typical AP firing evoked by sustained input currents (− 0.2 and + 0.55 nA; bars: 25 mV; 250 ms) and relevant raster plots (I_{inj} range: + 0.2 and + 0.6 nA) depicting evident depolarization-block (arrow) in 3 months-old Tg CA1 neurons. Right, Pooled data of the threshold current for DB ($_{MIN}I_{inj}$). Note that in Tg mice the block occurs already at 3 months of age (** $p = 0.0086$ vs WT, Mann Whitney test, 17 cells each) and is still present at 8 months of age (3- vs 8-month Tg: $p = 0.7402$, unpaired t-test with Welch's correction). At difference, DB appears in WT neurons at older age only (3- vs 8-month WT, ** $p = 0.0011$, Mann Whitney test), when WT and Tg mice bear similar block (at 8 months of age, Tg vs WT: $p = 0.6209$, unpaired t-test with Welch's correction, 12 cells each). C, mAHP analysis. Left, example traces showing potentiation of mAHP in Tg CA1 neurons (bars: 25 mV; 250 ms; inset: 5 mV; 25 ms). Right, Pooled data: at 3 months, WT vs Tg *** $p = 0.0004$, 17 cells each; at 8 months, WT vs Tg $p = 0.2092$, 13 cells each. No changes were found for mAHP along development (WT $p = 0.3890$ and Tg $p = 0.1655$). All unpaired t-test with Welch's correction.

3.2. Firing alterations in ventral CA1 pyramidal neurons of Tg2576 mice show early onset

In animal models, some decrease of AP firing rate in CA1 pyramidal cells is a hallmark of physiological aging (Landfield and Pitler, 1984; Randall et al., 2012) and, when exacerbated, of AD (Cordella et al., 2018; Kaczorowski et al., 2011; Pousinha et al., 2019; see also Fig. 1B). We thus asked whether in the Tg2576 mouse model ventral CA1 neurons also suffer from an accelerated rundown of their firing performance with age, compared to WTs.

To investigate this, we compared *f* – I relationships within strains and along development (rather than across strains at fixed age-points). For WT neurons, we found that the input-output curves underwent relevant changes with age (Fig. 2A): first, the average curve in older mice shifted to the left (within the analysed range of I_{inj}: WT 3-months vs 8- months, $p = 0.0304$, $F_{1,27} = 5.220$); this was in agreement with the age-dependent decrease of the rheobase in WTs (see Fig. 1A). Secondly, only CA1 neurons from younger WTs could respond to increasing current injections with sustained firing, whilst neurons in older mice partially lost this ability, showing significant reduction of their firing

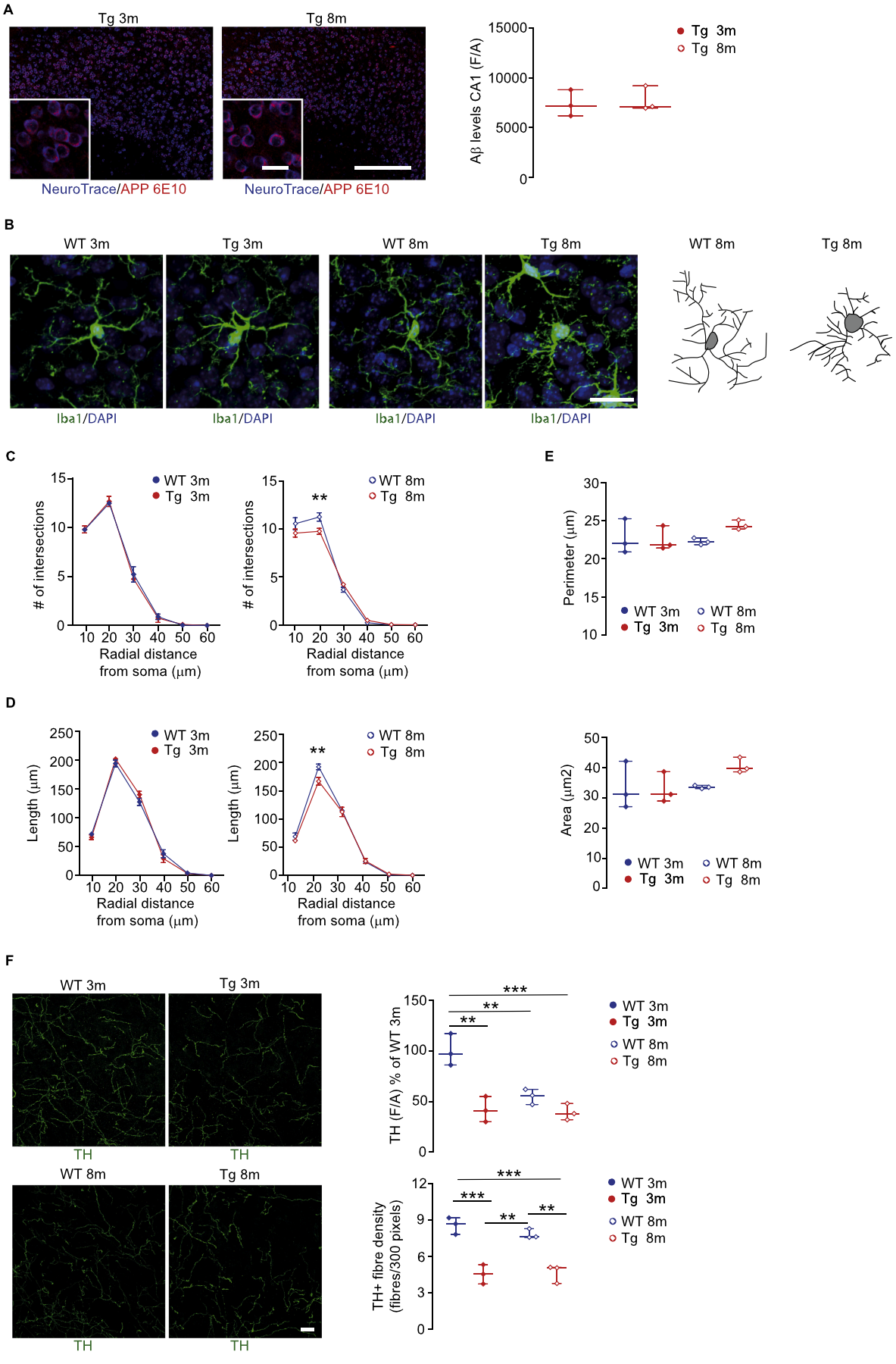

(caption on next page)

Fig. 3. Early reduction of TH^+ fibre density in the ventral CA1 of Tg2576 mice occurs in absence of Aβ plaques or neuroinflammation. A, Left, NeuroTrace/APP 6E10 staining in the ventral CA1 region of 3 and 8 months-old Tg mice (scale bar: 250 μm, inset 25 μm); Right, scatter plot of mean (± s.e.m) Aβ levels (3 mice per group; unpaired t-test with Welch's correction, $p = 0.7467$). B, Z-stack double-labelling of Iba1 and DAPI in the ventral CA1 hippocampus of 3 and 8 months-old WT and Tg mice (scale bar: 20 μm) and representative 3D-reconstructed microglia used for Sholl analysis. C-E, Morphological complexity of $Iba1^+$ cells, depicted by (C) number of intersections and (D) length of processes along radial distance from the soma, as well as by (E) soma perimeter (top) and area (bottom), in 3 and 8 months-old mice (mean ± s.e.m.; 3 animals per group; 5 sections per animal; *intersections 3 m*: 2-way RM ANOVA interaction $F_{5,20} = 0.244$, $p = 0.938$; radial distance $F_{5,20} = 517.9$, $p < 0.0001$; genotype $F_{1,4} = 0.068$, $p = 0.3387$; *intersections 8 m*: 2-way RM ANOVA interaction $F_{5,20} = 3.58$, $p = 0.0178$; radial distance $F_{5,20} = 566$, $p < 0.0001$; genotype $F_{1,4} = 5.76$, $p = 0.074$; Bonferroni's post-hoc: WT vs Tg: ** $p = 0.0057$ at 20 μm; *length 3 m*: 2-way RM ANOVA interaction $F_{5,20} = 1.66$, $p = 0.1890$; radial distance $F_{5,20} = 635.3$, $p < 0.0001$; genotype $F_{1,4} = 0.124$, $p = 0.7430$; *length 8 m*: 2-way RM ANOVA interaction $F_{5,20} = 2.96$, $p = 0.0370$; radial distance $F_{5,20} = 544$, $p < 0.0001$; genotype $F_{1,4} = 7.139$, $p = 0.056$; WT vs Tg: ** $p = 0.0014$ at 20 μm; *soma perimeter*: 2-way ANOVA interaction $F_{1,8} = 2.03$, $p = 0.1921$; age $F_{1,8} = 0.77$, $p = 0.4062$; genotype $F_{1,8} = 1.41$, $p = 0.2689$; *soma area*: 2-way ANOVA interaction $F_{1,8} = 1.807$, $p = 0.2161$; age $F_{1,8} = 1.94$, $p = 0.2000$; genotype $F_{1,8} = 1.34$, $p = 0.278$). F, To the left, Z-stack immunofluorescent labelling of TH^+ fibres of ventral CA1 (scale bar: 20 μm). The upper scatter plot depicts densitometric values of TH (± s.e.m.; expressed as % of WT 3 m levels) in 3- and 8 months-old WT and Tg mice (3 mice per group, 5 sections per animal; 2-way ANOVA interaction $F_{1,8} = 10.21$, $p = 0.0127$; age $F_{1,8} = 12.95$, $p = 0.0071$; genotype $F_{1,8} = 30.93$, $p = 0.0005$; Tukey's post-hoc test: 3 m WT vs 3 m Tg: ** $p = 0.0012$; 3 m WT vs 8 m WT: ** $p = 0.0059$; 3 m WT vs 8 m Tg: *** $p = 0.0009$); the bottom plot shows mean of TH^+ fibre density (fibres/300 pixels) in the ventral CA1 (± s.e.m.; 3 mice per group, at least 4 sections per animal; 2-way ANOVA interaction $F_{1,8} = 1.191$, $p = 0.307$; age $F_{1,8} = 0.639$, $p = 0.4473$; genotype $F_{1,8} = 84.92$, $p < 0.0001$; Tukey's post-hoc: 3 m WT vs 3 m Tg: *** $p = 0.0004$; 3 m WT vs 8 m Tg: *** $p = 0.0005$; 3 m Tg vs 8 m WT: ** $p = 0.0015$; 8 m WT vs 8 m Tg: ** $p = 0.0019$).

rate (for I_{inj} + 0.6 nA, $p = 0.0364$; Fig. 2A).

When analysing Tg2576 firing along age progression, rather than an analogous or worsened age-dependent alteration of the evoked firing, to some surprise we found that the $f - I$ relationships were almost completely superimposable ($p = 0.8473$, $F_{1,27} = 0.0378$; Fig. 2A). Thus, ventral CA1 neurons of younger Tg2576 mice not only lack the increase of cell excitability observed in WTs along development, but also, and importantly, show anticipated inability to bear sustained firing, a deficit typical of elder WT mice (Fig. 2A).

By inspecting the current-clamp recordings we could readily acknowledge that neurons with deficient firing had features typical of the depolarization-block (DB), during which the number of APs drops and the membrane voltage reaches an equilibrium value of approx. – 40 mV or more (Bianchi et al., 2012; Fig. 2B). We quantified DB by estimating the threshold current for the depolarization-block (that is, the minimal amount of injected current needed to reach the maximal firing frequency observed, $_{MIN}I_{inj}$; Bianchi et al., 2012) and found that indeed neurons from Tg2576 mice undergo DB earlier than WTs and at significantly lower values of $_{MIN}I_{inj}$ (at 3-months, WT 0.51 ± 0.02 nA and Tg2576 0.39 ± 0.04 nA, $p = 0.0086$; at 8-months, WT 0.35 ± 0.04 nA and Tg2576 0.38 ± 0.03 nA, $p = 0.6209$; Fig. 2B). Thus, as expected from the rundown of firing performance with age (see Fig. 2A), WT pyramidal neurons showed depolarization-block in older animals, which was anticipated at 3 months of age in Tg2576 mice ($_{MIN}I_{inj}$: WT 3-m vs 8-m, $p = 0.0011$; Tg2576 3-m vs 8-m, $p = 0.7402$; Fig. 2B).

Afterhyperpolarization (AHP) following one or more APs is known to be a key regulator of neuronal homeostatic firing in general (Disterhoft and Oh, 2007; Moyer et al., 1992; Storm, 1987, 1990) and is critical for controlling the excitability of pyramidal neurons both in young and aging hippocampus (Disterhoft and Oh, 2007; Disterhoft et al., 1996; Landfield and Pitler, 1984; Oh et al., 2016). Although the actual contribution of different ionic conductances to AHP is debated (see Gu et al., 2005; Hammond et al., 2006), voltage- and/or Ca^{2+}- sensitive potassium channels are involved. Recently the expression of intracellular APP in dorsal CA1 has been correlated to the modulation of Ca^{2+} influx and consequently to the potentiation of postburst AHP (Pousinha et al., 2019). Here, we asked whether the AHP of ventral CA1 neurons was different in Tg2576 mice and found that the $mAHP_{peak}$ was significantly potentiated in Tg2576 animals of 3 months (3-months: WT – 2.1 ± 0.3 mV and Tg2576 – 4.3 ± 0.4 mV, $p = 0.0004$; 8-months: WT – 2.6 ± 0.4 mV and Tg2576 – 3.4 ± 0.5 mV, $p = 0.2092$; Fig. 2C). This finding suggested that the modulation of voltage- or Ca^{2+}- sensitive ion channels could play a role in the altered firing of Tg2576 ventral CA1 neurons.

Altogether our current-clamp analysis suggests that in Tg2576 mice the pyramidal neurons of the ventral CA1 suffer from early deterioration of their excitability, thus largely before the appearance of typical AD-related markers such as Aβ plaques or neuroinflammation. Indeed, we confirmed the presence of only intracellular Aβ in ventral CA1 neurons, which remained at comparable levels in 8-months old animals, in line with the relatively slow disease progression typical of this AD model (Fig. 3A; Suppl. Fig. 2A). Also, at 3 months of age no signs of neuroinflammation were present, as suggested by the unaltered morphological profile of resident $Iba1^+$ microglial cells (which showed slight, but significant alteration of their proximal branching only in 8-months old Tg2576 mice; Fig. 3B-E; Suppl. Fig. 2B).

Instead, and intriguingly, the early deterioration of excitability in ventral CA1 pyramidal cells temporally coincides with the initial loss of VTA dopaminergic neurons, which starts between 2 and 3 months of age in this AD model, as previously reported (Nobili et al., 2017). We thus pursued the possibility that the impaired excitability borne by CA1 neurons could relate to a lower presence of DA in the VTA projections reaching the ventral hippocampus. To ascertain this, we performed densitometric analysis of TH – the rate-limiting enzyme for DA production – and found that indeed it was strongly reduced in Tg2576 mice (at both 3- and 8-months of age) as well as in 8-months old WT mice compared to 3-months old WTs (Fig. 3F). In particular, TH expression was significantly lower in the ventral CA1 of 3-months old Tg mice compared to WTs of the same age ($p = 0.0012$) and remained equally low in older Tg mice ($p = 0.9913$). Notably, we also observed a significant reduction of TH levels in 8-months old WT mice compared to younger WTs ($p = 0.0059$), that was however not due to a reduction in TH^+ fibre density (Fig. 3F). Thus, overall the quantification of TH levels in the ventral CA1 along ages and across strains mirrored both the reduction of neuronal rheobase (Fig. 1) and the modification of firing properties of ventral CA1 neurons along time (Fig. 2), strongly suggesting the existence of a causative link between the two phenomena.

3.3. CA3 – CA1 synapse strength of ventral Tg2576 CA1 pyramidal cells is unaltered

We and others reported that Tg2576 mice older than 5–6 months of age show impairment of the hippocampal memory, observed both at behavioural and cellular level in dorsal dentate gyrus, CA3 – CA1 and CA1 – preSub synaptic plasticity (Chapman et al., 1999; Cordella et al., 2018; Corsetti et al., 2020; Jacobsen et al., 2006; Nobili et al., 2017; Taglialatela et al., 2009). As soon as at 3 months of age however, Tg2576 mice start showing behavioural deficits (fear conditioning performance) reflecting functional (decreased evoked EPSCs and mEPSC frequency), structural (lower spine density and size of dorsal CA1 pyramidal neurons) and biochemical (lower hippocampal GluA1 levels) alterations (Cavallucci et al., 2013a, 2013b; D'Amelio et al., 2011). Thus, we asked whether analogous alterations affected the ventral CA1 of Tg2576 mice. To address this, firstly we recorded spontaneous excitatory synaptic currents from CA1 pyramidal neurons of Tg2576 and WT animals. In line with other reports for this and other AD models (Chapman et al., 1999; Cordella et al., 2018; Neuman et al., 2015), we found that the

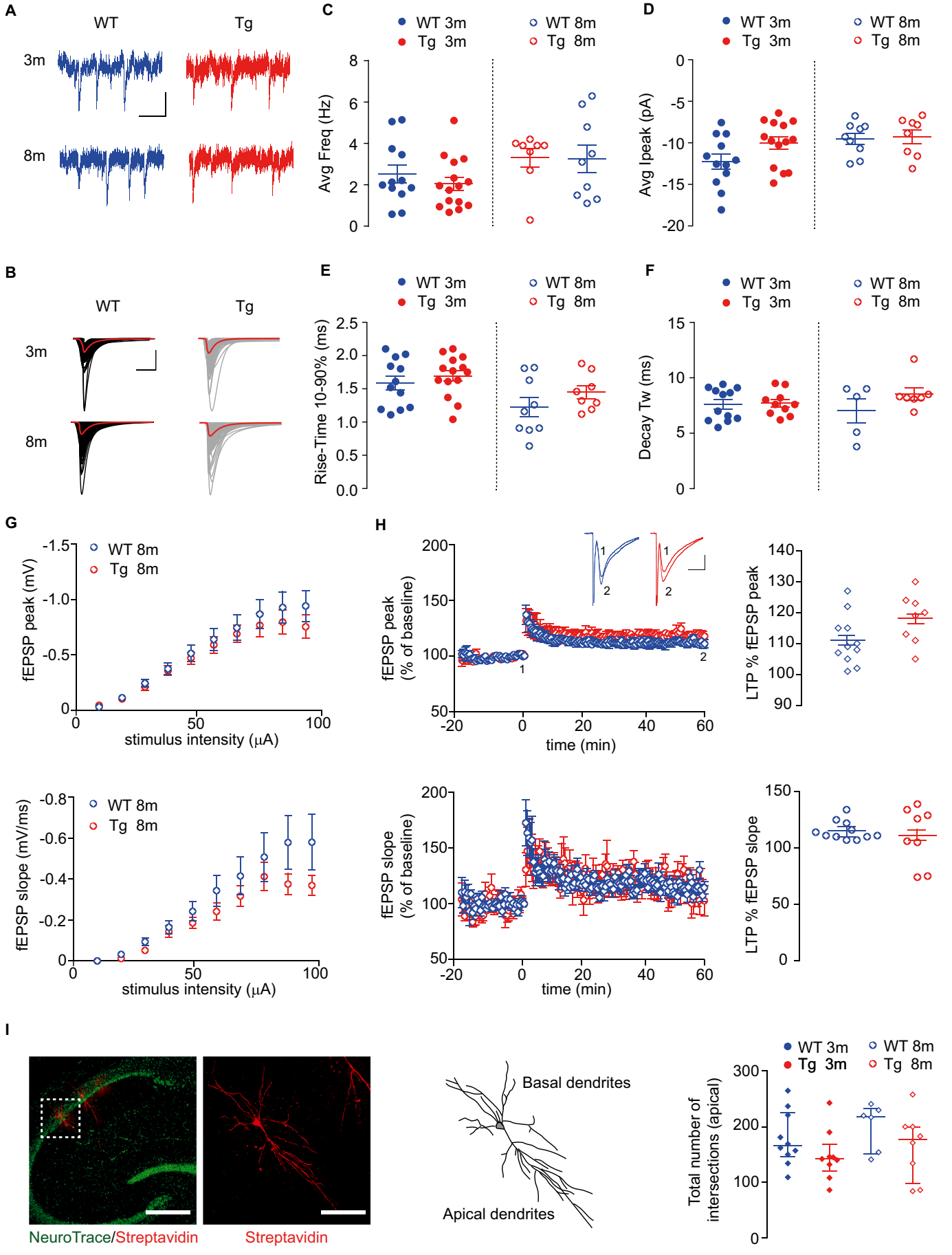

(caption on next page)

Fig. 4. Spontaneous excitatory (CA3 – CA1) synaptic drive onto ventral CA1 neurons, LTP and apical dendrite branching are unaltered in Tg mice. A, Typical traces showing sEPSCs recorded at − 70 mV from CA1 neurons of WT or Tg mice of 3 or 8 months of age. Traces were post-hoc filtered (f_c 1 kHz) for clarity. Scale bars: 10 pA; 250 ms. B, Populations of the three-exponential fits (and superimposed average fit, red) used for sEPSC analysis. Scale bars: 20 pA; 20 ms. C - F Scatter plots depicting lack of differences across strains at different ages. In details, average sEPSC frequency: *at 3 months*, WT 2.5 ± 0.4 Hz (12 cells, 4 mice; 2699 events); Tg 2.1 ± 0.3 Hz (15 cells, 6 mice; 2941 events; $p = 0.4036$; unpaired t-test with Welch's correction); *at 8 months*, WT 3.3 ± 0.7 Hz (9 cells, 3 mice; 2868 events); Tg 3.3 ± 0.5 Hz (8 cells, 2 mice; 2446 events; p = 0. 7422; Mann Whitney test). Average I_{peak}: at 3 months, WT – 12.3 ± 0.9 pA (12 cells, 4 mice; 2543 events); Tg – 10.0 ± 0.7 pA (14 cells, 6 mice; 2505 events; $p = 0.0667$; unpaired t-test with Welch's correction); at 8 months, WT – 9.5 ± 0.7 pA (9 cells, 2 mice; 2591 events); Tg – 9.3 ± 0.8 pA (8 cells, 2 mice; 1991 events; $p = 0.8137$; unpaired t-test with Welch's correction). Average 10–90% rise-time: at 3 months, WT 1.6 ± 0.1 ms (12 cells, 4 mice; 2543 events); Tg 1.70 ± 0.08 ms (14 cells, 6 mice; 2505 events; $p = 0.4090$; unpaired t-test with Welch's correction); at 8 months, WT 1.2 ± 0.1 ms (9 cells, 2 mice; 2591 events); Tg 1.5 ± 0.1 ms (8 cells, 2 mice; 1991 events; $p = 0.2218$; unpaired t-test with Welch's correction). Average decay T_w: at 3 months, WT 7.6 ± 0.4 ms (12 cells, 4 mice; 2539 events); Tg 7.7 ± 0.4 ms (10 cells, 5 mice; 1262 events; $p = 0.8695$; unpaired t-test with Welch's correction); at 8 months, WT 7 ± 1 ms (5 cells, 2 mice; 949 events); Tg 8.6 ± 0.6 ms (7 cells, 2 mice; 1880 events; $p = 0.9066$; Mann Whitney test). G, Input-output curves of CA3-CA1 fEPSP peak (top) and slope (bottom) in response to stimuli of increasing intensity, recorded from 8 months-old WT or Tg mice (WT 11 slices from 6 mice; Tg 8 slices from 5 mice). No differences were observed between genotypes (peak, $p = 0.9915$, $F_{9,166} = 0.2188$; slope, $p = 0.9037$, $F_{9,165} = 0.4533$ with 2-way ANOVA). H, Time-course of normalised, average fEPSP peak (top) and slope (bottom) from WT and Tg mice depicting same synaptic potentiation in both strains. Traces show typical fEPSPs recorded during baseline and 1 h after the conditioning train (scale bars: 0.5 mV; 20 ms). Right, pooled data for fEPSP normalised peak ($p = 0.0763$) and slope ($p = 0.6682$; both unpaired t-test with Welch's correction). I, Z-stack double-labelling of NeuroTrace/Streptavidin of biocytin-filled CA1 pyramidal neurons in the ventral hippocampus (left; scale bar: 200 μm) with magnification of a single neuron (scale bar: 50 μm) and its 3D-reconstruction used for Sholl analysis; to the right the scatter plot of mean (± s.e.m) total number of apical dendrite intersections of pyramidal neurons across genotypes and ages (2 animals per group, WT 3 m $n = 10$; Tg 3 m $n = 9$; WT 8 m $n = 6$; Tg 8 m $n = 8$ cells; 2-way ANOVA: interaction $F_{1,29} = 0.024$, $p = 0.8772$; age $F_{1,29} = 1.19$, $p = 0.2843$; genotype $F_{1,29} = 3.55$, $p = 0.0696$). (For interpretation of the references to colour in this figure legend, the reader is referred to the web version of this article.)

spontaneous release at the CA3 – CA1 synapse recorded in presence of pre-synaptic APs was unaltered in these mice, both at 3 and 8 months of age. Thus, sEPSCs recorded from WT and Tg2576 CA1 neurons had same average frequency, peak current and kinetics (Fig. 4A-F).

Secondly, we investigated whether the evoked long-term plasticity at these synapses of the ventral hippocampus was defective, similarly to what reported for the dorsal area in 8 months-old animals (Cordella et al., 2018; Nobili et al., 2017). In line with what we previously observed for the dorsal hippocampus (Nobili et al., 2017) and with what we expected from our sEPSC data, the fEPSP input-output relationship was similar between 8 months-old WT and Tg2576 mice, further confirming lack of change in basal glutamatergic transmission across genotypes (Fig. 4G). Interestingly however, at odds with the dorsal hippocampus we found no difference in CA3 – CA1 LTP between WT and Tg2576 animals (fEPSP normalised peak: WT 111 ± 2% and Tg2576 118 ± 3%, $p = 0.0763$; fEPSP normalised slope: WT 115 ± 3% and Tg2576 111 ± 9%; $p = 0.6682$; Fig. 4H). Thus, albeit ventral CA1 pyramidal neurons in Tg2576 mice had derailed firing since early stages of their development, both excitatory basal synaptic transmission and plasticity in this area were intact. To validate our functional observations, we performed morphometric analysis of the branching of pyramidal neuron dendrites in the stratum radiatum. In fact, Sholl analysis of biocytin-filled neurons showed similar number of total apical intersections in WT and Tg2576 neurons, irrespective of the mouse age (Fig. 4I, Suppl. Fig. 2C); this finding is in line with our electrophysiological results (Fig. 4A-H).

3.4. Computational modelling of excitability alterations in ventral CA1 pyramidal neurons of Tg2576 mice

To shed some light on the possible mechanisms underlying the altered excitability and, specifically, the early onset of depolarization block found in ventral CA1 neurons of younger Tg2576 mice, we modelled the passive properties and the firing behaviour of representative recorded neurons in each condition. The optimized values of channel conductance in modelled neurons were compared *across* strains at the two age points studied (3- and 8- months; Fig. 5), as well as *within* strains, to find possible channel modulations underlying the different maturation of the firing profile in the two mouse strains along development (Suppl. Fig. 3).

The modelling supported the view that altered firing and impaired development of excitability in pyramidal cells of the ventral CA1 of Tg2576 mice start at a very early, pre-plaque phase of the disease. In details, the models suggested that anticipated appearance of DB in Tg2576 neurons could be related to the decrease of the K_{DR} channel conductance density (Fig. 5A). At 8 months of age, when Tg2576 CA1 neurons showed apparent reduced excitability compared to WTs (see Fig. 1), the computational analysis indicated that a significant increase of the peak conductance for K_{Ca} channels would lead to the lower AP frequency observed (Fig. 5B).

Both these conductances changed in Tg2576 mice when comparing model results for younger vs older neurons (Suppl. Fig. 3). Altogether, our computational study suggested that both a shift of sodium channel activation kinetics in the main compartments of modelled neurons (Bianchi et al., 2012; see Methods) and the alteration of K_{DR} and K_{CA} potassium conductances were required to predict the derailed firing behaviour found experimentally in younger and older CA1 pyramidal neurons in the ventral hippocampus of Tg2576 model mice.

4. Discussion

We provide evidence that pyramidal cells in the ventral CA1 of the Tg2576 mouse model of AD present altered firing and impaired excitability since very early phases of the disease. Also, we indicate the depolarization block and derailment of specific conductances (I_{Na}; K_{DR}; K_{Ca}) as possible ionic mechanisms underlying such early alteration. Finally, we highlight that even in the presence of such derailments, basal transmission and long-term potentiation at ventral CA3 – CA1 synapses remain unaltered compared with age-matched controls. Previously, we had demonstrated that dorsal CA1 and pre-Sub of these mice bear profound alteration of both neuron excitability and glutamatergic synaptic transmission and plasticity, leading to impaired excitatory inputs onto the NAc *core* (Cordella et al., 2018; Nobili et al., 2017). Together, our previous and new findings depict how pyramidal neurons of both dorsal and ventral main output of hippocampal circuitry are profoundly, and yet somehow distinctly, altered in Tg2576 animals since pre-plaque stages of AD.

Reduced evoked excitability and increased spike V_{thre} found in ventral CA1 of 8 months-old mice are in line with data previously obtained in the dorsal pre-Sub of these animals at the same disease stage (Cordella et al., 2018). Thus, in both regions some early event (or chain of events) is able to undermine the fine-tuning of AP firing in CA1 pyramidal neurons. Here we tackled such early events in the ventral CA1 and identified two properties of pyramidal cells that physiologically are associated with aging but appear earlier than normal in Tg2576 mice: reduced rheobase (Fig. 1) and depolarization-block of firing (Fig. 2).

Homeostatic control of firing contributes synergistically with synaptic plasticity to information storage in neuronal networks and memory (Debanne and Poo, 2010; LeMasson et al., 1993; Turrigiano, 2011; Turrigiano et al., 1998). Dysregulation of this balance is now considered

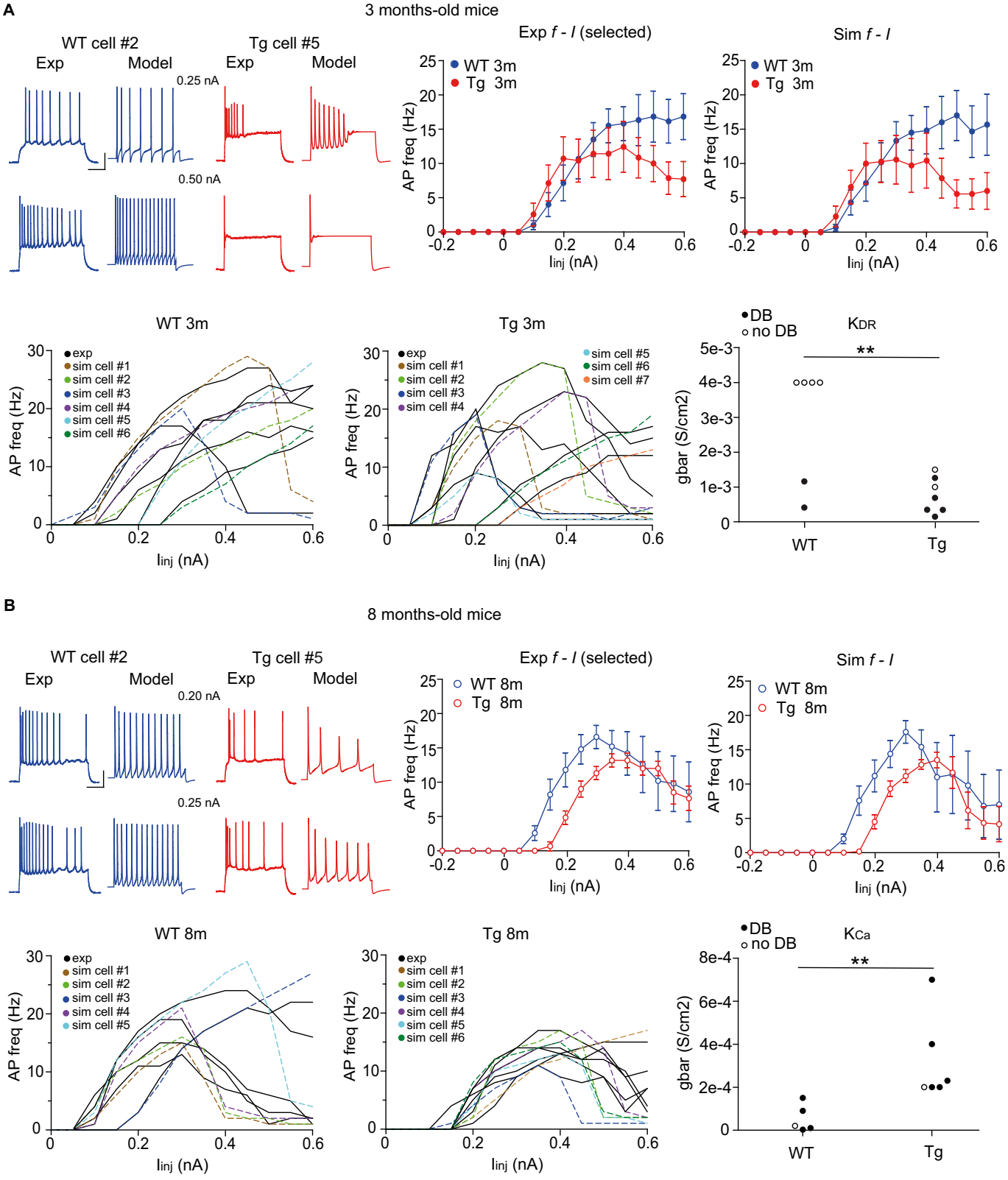

Fig. 5. Computational modelling of electrophysiological features of ventral CA1 pyramidal neurons. A, Typical experimental and modelled somatic voltage response to current injections in neurons of 3 months-old WT or Tg mice (upper left; bars: 25 mV; 250 ms) and mean *f - I* relationships for selected neurons (upper right). *f - I* curves for each neuron (simulation vs recorded) are also shown, to depict modelling accuracy (lower left panels: black lines identify experimental data, colored dashed lines represent simulations). According to our computational analysis, the early appearance of depolarization block observed in CA1 neurons from 3-months old Tg mice could be ascribed to a significant decrease of conductance density for K_{DR} channels in these neurons ($p < 0.001$ vs WT; lower right; open symbols depict neurons not entering the DB state; filled symbols, neurons entering DB). B, Same as in A, for neurons from 8 months-old WT or Tg mice. In this case, our computational analysis suggested that the different *f - I* relationships observed in Tg mice could be due to a significantly increased peak conductance for K_{Ca} channels ($p = 0.004$ vs WTs; lower right).

a major cause of memory impairments in early AD (reviewed in Styr and Slutsky, 2018). Thus, synapse weakening and memory deficits could stem from chronic firing abnormalities, in case compensatory mechanisms fail. CA1 pyramidal cells (like other neurons) can plastically adapt several of their electrophysiological properties to accommodate for modifications of the environment - a property of complex biological system called *degeneracy* (Drion et al., 2015; Edelman and Gally, 2001). Modelling studies suggest that in CA1 neurons only few conductances (e.g. somatic K_M, I_h and dendritic K_{DR}) are so crucial to neuronal survival to be normally excluded from degeneracy (Migliore et al., 2018): alterations affecting these channels would unlikely come without a cost. Intriguingly, among these key conductances, K_M is central in controlling pyramidal excitability (Gu et al., 2005; but see Chen et al., 2014; reviewed in Marrion, 1997), and K_{DR} (together with I_{Na}) is most involved with the generation of DB (Bianchi et al., 2012) – the two conductances we found altered in young Tg2576 neurons of the ventral CA1. Thus, we hypothesized that some early, persistent perturbation of key conductances could disrupt the homeostatic control of AP firing in Tg2576 ventral CA1 neurons and eventually their ability to pass the upstream information to downstream networks with high fidelity. Our hypothesis is supported by the observation that, indeed by altering kinetic properties and conductance distribution of K_{DR} and K_{Ca} (and transient I_{Na}), we could satisfactorily model the firing alterations observed experimentally.

What is the nature of such initial perturbation? It is worth noting that the early alterations found here in the ventral CA1 of 3-month-old Tg2576 mice are timely with the first detectable degeneration of the VTA DA neurons in this AD model mouse (La Barbera et al., 2021; Nobili et al., 2017). Of note, we and others had previously shown that excitability, synaptic and behavioural deficits found in older Tg2576 animals could be rescued by sub-chronic intraperitoneal administration of L-DOPA (Ambrée et al., 2009; Cordella et al., 2018; Jürgensen et al., 2011; Nobili et al., 2017), suggesting that the loss of DA tone in the hippocampus following DA neuron degeneration is directly linked to excitability changes. Similarly, Edelmann and Lessmann (2011) demonstrated that acute inhibition of D1-mediated signalling altered APs and time-dependent CA3 – CA1 LTP in pyramidal neurons; again, these alterations could be rescued by acute administration of physiological concentrations of DA (20 μM; Edelmann and Lessmann, 2011). All these evidences point at lower levels of DA as a possible trigger of the early, pre-plaque alterations found in AD models. Indeed, here we confirmed that the dopaminergic innervation in the ventral hippocampus is reduced in Tg2576 mice already since 3 months of age, in line with the early derailment of pyramidal neuron properties. Furthermore, we observed that a reduction of TH levels is also occurring in older (8-months) WT animals (see also Collier et al., 2007; Irwin et al., 1994; Norrara et al., 2018). Yet, unlike Tg2576 mice, the reduction of TH levels in older WTs is not due to degeneration of DA neurons in the VTA (see Nobili et al., 2017), not due to the loss of TH fibres in the ventral hippocampus (see Fig. 3F). We can assume that the reduction of DA levels in mature WT animals is a physiological process occurring in parallel with age-dependent changes in dopaminergic neuron firing (McCutcheon et al., 2012) and the consequent changes in TH levels (Aumann et al., 2011). Thus, in older WTs (8-months), despite the absence of AD-promoting factors like Aβ or neuroinflammation, lower DA levels might start contributing to the observed first signs of reduced firing in ventral CA1 neurons. This, in turn, would obviously appear even worse in 8-months old Tg2576 mice (see for example the even lower neuronal excitability compared to aged-matched WTs, Fig. 1A-C) due to the progressive degeneration of DA neurons in the VTA and the concurrence with AD factors like chronic presence of Aβ or neuroinflammation.

Accordingly, DB and derailment of action potential firing in hippocampal pyramidal neurons, as well as changes in the AHP and intracellular calcium buffering, are common features between aging mice (Gant et al., 2015; Moyer et al., 1992; Oh et al., 2016; Randall et al., 2012) and Tg2576 mice as shown here and reported previously (Cordella et al., 2018). Such age-dependent alterations usually reflect into changes of animal behaviour, including worsening of cognitive performance (Gant et al., 2015; Potier et al., 1992). Given the well-characterized role of DA in cognitive functions (Bethus et al., 2010; Broussard et al., 2016; McNamara et al., 2014; Rossato et al., 2009; Yang et al., 2017), it seems reasonable to assume that the progressive loss of TH levels in the hippocampus of Tg2576 mice can contribute to the cognitive dysfunctions described in this AD model (La Barbera et al., 2021; Nobili et al., 2017).

Interestingly, our study also highlighted the somehow striking difference emerged when comparing the modifications of synaptic plasticity in ventral and dorsal hippocampus in 6–8 months old Tg2576 animals: dorsal synapses (CA3 – CA1 and CA1 – preSub) and dendritic spines are all equally affected (Cordella et al., 2018; D'Amelio et al., 2011; Nobili et al., 2017), whilst ventral CA3 – CA1 transmission and apical dendrite branching appear to be preserved (see Fig. 4). This finding is not completely surprising given our growing understanding of functional distinctions between dorsal and ventral hippocampus (Kheirbek et al., 2013; Strange et al., 2014) and is in line with observations showing that DA receptors are differentially distributed along the dorso-ventral axis in the rodent brain (Dubovyk and Manahan-Vaughan, 2019) or that the VTA sends more dopaminergic projections to the ventral than to the dorsal hippocampus (Kempadoo et al., 2016). In this scenario, it seems acceptable to speculate that the apparent lack of changes in synaptic plasticity in the ventral CA1 might depend on the presumably larger dopaminergic tone present in this sub-region, even in the presence of degeneration of the VTA in Tg2576 animals. At the same time, the stronger alterations that we and others have previously reported for the dorsal hippocampus might depend on the loss of a relatively small, yet critical level of dopaminergic control from the VTA or, alternatively, on alterations of the dopaminergic/noradrenergic projections reaching from the locus coeruleus, an aspect worth investigating in detail (for a review see Krashia et al., 2019b; Sara, 2009; see also Caligiore et al., 2020).

In conclusion, CA1 pyramidal neurons in the ventral hippocampus of Tg2576 mice show late depression of evoked excitability and depolarised V_{thre} for APs as well as early onset of depolarization-block compared to WT neurons, whilst CA3 – CA1 plasticity stays intact. These alterations are timely with loss of dopaminergic neurons of the VTA in this AD model. We thus hypothesize that reduction of homeostatic levels of extracellular DA plays a role in triggering the loop of neuronal derailment eventually leading to hippocampal decline.

Author contributions

ES, PK and MR performed the electrophysiological experiments and analysed the data. CAL, EG, and MM performed computational analysis and simulations. LLB and AN performed morphometric and immunofluorescence analysis. PK, MR and MDA conceived the experiments. MR wrote the manuscript, with the collaboration of PK, MM and MDA. All authors discussed the data and approved the final version of the manuscript.

Funding

ES was supported by a PhD fellowship by Fondazione Melchiorri (IT). PK was supported by an under-40 grant from the Italian Association for Alzheimer's Research (AIRALTZH-AGYR2020). MM, CAL, and EG were supported by the EU Horizon 2020 Framework Program for Research and Innovation (Specific Grant 945539, Human Brain Project SGA3) and by the Flag ERA JTC 2019 (MILEDI Project). MM also acknowledges FENIX computing and storage resources under the Specific Grant Agreement No. 800858 (Human Brain Project ICEI), and a grant from the Swiss National Supercomputing Centre (CSCS) under projects ID ich011 and ich002. MDA was supported by the American Alzheimer's

Association (AARG-18-566270), by the Italian Ministry of Health (Research Grant: RF-2018 -12365527) and by Fondazione Roma (Rome, Italy).

Declaration of Competing Interest

The authors declare that they have no known competing financial interests or personal relationships that could have appeared to influence the work reported in this paper.

Acknowledgements

We are deeply grateful to Dr. Maria Teresa Viscomi for her valuable help with data analysis, Dr. Francescangelo Vedele for helping with slice preparation and Drs Riviello and Wirz for assistance with animal caring.

Appendix A. Supplementary data

Supplementary data to this article can be found online at https://doi.org/10.1016/j.expneurol.2021.113969.

References

Allard, P., Alafuzoff, I., Carlsson, A., Eriksson, K., Ericson, E., Gottfries, C.G., Marcusson, J.O., 1990. Loss of dopamine uptake sites labeled with [3H]GBR-12935 in Alzheimer's disease. Eur. Neurol. 30, 181–185.
Ambrée, O., Richter, H., Sachser, N., Lewejohann, L., Dere, E., de Souza Silva, M.A., Herring, A., Keyvani, K., Paulus, W., Schäbitz, W.-R., 2009. Levodopa ameliorates learning and memory deficits in a murine model of Alzheimer's disease. Neurobiol. Aging 30, 1192–1204.
Ascoli, G.A., 2006. Mobilizing the base of neuroscience data: the case of neuronal morphologies. Nat. Rev. Neurosci. 7, 318–324.
Aumann, T.D., Egan, K., Lim, J., Boon, W.C., Bye, C.R., Chua, H.K., Baban, N., Parish, C. L., Bobrovskaya, L., Dickson, P., et al., 2011. Neuronal activity regulates expression of tyrosine hydroxylase in adult mouse substantia nigra pars compacta neurons. J. Neurochem. 116, 646–658.
Ballard, C., Gauthier, S., Corbett, A., Brayne, C., Aarsland, D., Jones, E., 2011. Alzheimer's disease. Lancet 377, 1019–1031.
Bateman, R.J., Xiong, C., Benzinger, T.L.S., Fagan, A.M., Goate, A., Fox, N.C., Marcus, D. S., Cairns, N.J., Xie, X., Blazey, T.M., et al., 2012. Clinical and biomarker changes in dominantly inherited Alzheimer's disease. N. Engl. J. Med. 367, 795–804.
Bean, B.P., 2007. The action potential in mammalian central neurons. Nat. Rev. Neurosci. 8, 451–465.
Bethus, I., Tse, D., Morris, R.G.M., 2010. Dopamine and memory: modulation of the persistence of memory for novel hippocampal NMDA receptor-dependent paired associates. J. Neurosci. 30, 1610–1618.
Bianchi, D., Marasco, A., Limongiello, A., Marchetti, C., Marie, H., Tirozzi, B., Migliore, M., 2012. On the mechanisms underlying the depolarization block in the spiking dynamics of CA1 pyramidal neurons. J. Comput. Neurosci. 33, 207–225.
Blennow, K., de Leon, M.J., Zetterberg, H., 2006. Alzheimer's disease. Lancet 368, 387–403.
Broussard, J.I., Yang, K., Levine, A.T., Tsetsenis, T., Jenson, D., Cao, F., Garcia, I., Arenkiel, B.R., Zhou, F.-M., De Biasi, M., et al., 2016. Dopamine regulates aversive contextual learning and associated in vivo synaptic plasticity in the hippocampus. Cell Rep. 14, 1930–1939.
Caligiore, D., Silvetti, M., D'Amelio, M., Puglisi-Allegra, S., Baldassarre, G., 2020. Computational modeling of catecholamines dysfunction in Alzheimer's disease at pre-plaque stage. J. Alzheimers Dis. 77, 275–290.
Canter, R.G., Penney, J., Tsai, L.-H., 2016. The road to restoring neural circuits for the treatment of Alzheimer's disease. Nature 539, 187–196.
Cavallucci, V., Berretta, N., Nobili, A., Nisticò, R., Mercuri, N.B., D'Amelio, M., 2013a. Calcineurin inhibition rescues early synaptic plasticity deficits in a mouse model of Alzheimer's disease. NeuroMolecular Med. 15, 541–548.
Cavallucci, V., Ferraina, C., D'Amelio, M., 2013b. Key role of mitochondria in Alzheimer's disease synaptic dysfunction. Curr. Pharm. Des. 19, 6440–6450.
Chapman, P.F., White, G.L., Jones, M.W., Cooper-Blacketer, D., Marshall, V.J., Irizarry, M., Younkin, L., Good, M.A., Bliss, T.V., Hyman, B.T., et al., 1999. Impaired synaptic plasticity and learning in aged amyloid precursor protein transgenic mice. Nat. Neurosci. 2, 271–276.
Chen, S., Benninger, F., Yaari, Y., 2014. Role of small conductance Ca^{2+}-activated K^{+} channels in controlling CA1 pyramidal cell excitability. J. Neurosci. 34, 8219–8230.
Chételat, G., 2013. Alzheimer disease: Aβ-independent processes-rethinking preclinical AD. Nat. Rev. Neurol. 9, 123–124.
Collier, T.J., Lipton, J., Daley, B.F., Palfi, S., Chu, Y., Sortwell, C., Bakay, R.A.E., Sladek, J.R., Kordower, J.H., 2007. Aging-related changes in the nigrostriatal dopamine system and the response to MPTP in nonhuman primates: diminished compensatory mechanisms as a prelude to parkinsonism. Neurobiol. Dis. 26, 56–65.
Cordella, A., Krashia, P., Nobili, A., Pignataro, A., La Barbera, L., Viscomi, M.T., Valzania, A., Keller, F., Ammassari-Teule, M., Mercuri, N.B., et al., 2018. Dopamine loss alters the hippocampus-nucleus accumbens synaptic transmission in the Tg2576 mouse model of Alzheimer's disease. Neurobiol. Dis. 116, 142–154.
Corsetti, V., Borreca, A., Latina, V., Giacovazzo, G., Pignataro, A., Krashia, P., Natale, F., Cocco, S., Rinaudo, M., Malerba, F., et al., 2020. Passive immunotherapy for N-truncated tau ameliorates the cognitive deficits in two mouse Alzheimer's disease models. Brain Commun. 2, fcaa039.
D'Amelio, M., Rossini, P.M., 2012. Brain excitability and connectivity of neuronal assemblies in Alzheimer's disease: from animal models to human findings. Prog. Neurobiol. 99, 42–60.
D'Amelio, M., Cavallucci, V., Middei, S., Marchetti, C., Pacioni, S., Ferri, A., Diamantini, A., De Zio, D., Carrara, P., Battistini, L., et al., 2011. Caspase-3 triggers early synaptic dysfunction in a mouse model of Alzheimer's disease. Nat. Neurosci. 14, 69–76.
D'Amelio, M., Puglisi-Allegra, S., Mercuri, N., 2018a. The role of dopaminergic midbrain in Alzheimer's disease: Translating basic science into clinical practice. Pharmacol. Res. 130, 414–419.
D'Amelio, M., Serra, L., Bozzali, M., 2018b. Ventral tegmental area in prodromal Alzheimer's disease: bridging the gap between mice and humans. J. Alzheimers Dis. 63, 181–183.
De Marco, M., Venneri, A., 2018. Volume and connectivity of the ventral tegmental area are linked to neurocognitive signatures of Alzheimer's disease in humans. J. Alzheimers Dis. 63, 167–180.
Debanne, D., Poo, M.-M., 2010. Spike-timing dependent plasticity beyond synapse - pre- and post-synaptic plasticity of intrinsic neuronal excitability. Front. Synaptic Neurosci. 2, 21.
Disterhoft, J.F., Oh, M.M., 2007. Alterations in intrinsic neuronal excitability during normal aging. Aging Cell 6, 327–336.
Disterhoft, J.F., Thompson, L.T., Moyer, J.R., Mogul, D.J., 1996. Calcium-dependent afterhyperpolarization and learning in young and aging hippocampus. Life Sci. 59, 413–420.
Drion, G., O'Leary, T., Marder, E., 2015. Ion channel degeneracy enables robust and tunable neuronal firing rates. Proc. Natl. Acad. Sci. U. S. A. 112, E5361–E5370.
Dubovyk, V., Manahan-Vaughan, D., 2019. Gradient of expression of dopamine D2 receptors along the dorso-ventral axis of the hippocampus. Front. Synaptic Neurosci. 11, 28.
Edelman, G.M., Gally, J.A., 2001. Degeneracy and complexity in biological systems. Proc. Natl. Acad. Sci. U. S. A. 98, 13763–13768.
Edelmann, E., Lessmann, V., 2011. Dopamine modulates spike timing-dependent plasticity and action potential properties in CA1 pyramidal neurons of acute rat hippocampal slices. Front. Synaptic Neurosci. 3, 6.
Fanselow, M.S., Dong, H.-W., 2010. Are the dorsal and ventral hippocampus functionally distinct structures? Neuron 65, 7–19.
Gant, J.C., Chen, K.-C., Kadish, I., Blalock, E.M., Thibault, O., Porter, N.M., Landfield, P. W., 2015. Reversal of aging-related neuronal Ca2+ dysregulation and cognitive impairment by delivery of a transgene encoding FK506-binding protein 12.6/1b to the hippocampus. J. Neurosci. 35, 10878–10887.
Gibb, W.R., Mountjoy, C.Q., Mann, D.M., Lees, A.J., 1989. The substantia nigra and ventral tegmental area in Alzheimer's disease and Down's syndrome. J. Neurol. Neurosurg. Psychiatry 52, 193–200.
Gu, N., Vervaeke, K., Hu, H., Storm, J.F., 2005. Kv7/KCNQ/M and HCN/h, but not KCa2/SK channels, contribute to the somatic medium after-hyperpolarization and excitability control in CA1 hippocampal pyramidal cells. J. Physiol. 566, 689–715.
Guzmán-Ramos, K., Moreno-Castilla, P., Castro-Cruz, M., McGaugh, J.L., Martínez-Coria, H., LaFerla, F.M., Bermúdez-Rattoni, F., 2012. Restoration of dopamine release deficits during object recognition memory acquisition attenuates cognitive impairment in a triple transgenic mice model of Alzheimer's disease. Learn. Mem. 19, 453–460.
Hammond, R.S., Bond, C.T., Strassmaier, T., Ngo-Anh, T.J., Adelman, J.P., Maylie, J., Stackman, R.W., 2006. Small-conductance Ca2+−activated K+ channel type 2 (SK2) modulates hippocampal learning, memory, and synaptic plasticity. J. Neurosci. 26, 1844–1853.
Hao, J.-R., Sun, N., Lei, L., Li, X.-Y., Yao, B., Sun, K., Hu, R., Zhang, X., Shi, X.-D., Gao, C., 2015. L-Stepholidine rescues memory deficit and synaptic plasticity in models of Alzheimer's disease via activating dopamine D1 receptor/PKA signaling pathway. Cell Death Dis. 6, e1965.
Hardy, J., Selkoe, D.J., 2002. The amyloid hypothesis of Alzheimer's disease: progress and problems on the road to therapeutics. Science 297, 353–356.
Herrup, K., 2015. The case for rejecting the amyloid cascade hypothesis. Nat. Neurosci. 18, 794–799.
Himeno, E., Ohyagi, Y., Ma, L., Nakamura, N., Miyoshi, K., Sakae, N., Motomura, K., Soejima, N., Yamasaki, R., Hashimoto, T., et al., 2011. Apomorphine treatment in Alzheimer mice promoting amyloid-β degradation. Ann. Neurol. 69, 248–256.
Hines, M.L., Carnevale, N.T., 1997 Aug. The NEURON simulation environment. Neural Comput 159 (6), 1179–1209. https://doi.org/10.1162/neco.1997.9.6.1179. PMID: 9248061.
Hsiao, K., Chapman, P., Nilsen, S., Eckman, C., Harigaya, Y., Younkin, S., Yang, F., Cole, G., 1996. Correlative memory deficits, Abeta elevation, and amyloid plaques in transgenic mice. Science 274, 99–102.
Iaccarino, L., Sala, A., Caminiti, S.P., Presotto, L., Perani, D., Alzheimer's Disease Neuroimaging Initiative, 2020. In vivo MRI structural and PET metabolic connectivity study of dopamine pathways in Alzheimer's disease. J. Alzheimers Dis. 75, 1003–1016.
Irizarry, M.C., McNamara, M., Fedorchak, K., Hsiao, K., Hyman, B.T., 1997. APPSw transgenic mice develop age-related A beta deposits and neuropil abnormalities, but no neuronal loss in CA1. J. Neuropathol. Exp. Neurol. 56, 965–973.

Irwin, I., DeLanney, L.E., McNeill, T., Chan, P., Forno, L.S., Murphy, G.M., Di Monte, D. A., Sandy, M.S., Langston, J.W., 1994. Aging and the nigrostriatal dopamine system: a non-human primate study. Neurodegeneration 3, 251–265.
Jacobsen, J.S., Wu, C.-C., Redwine, J.M., Comery, T.A., Arias, R., Bowlby, M., Martone, R., Morrison, J.H., Pangalos, M.N., Reinhart, P.H., et al., 2006. Early-onset behavioral and synaptic deficits in a mouse model of Alzheimer's disease. Proc. Natl. Acad. Sci. U. S. A. 103, 5161–5166.
Joyce, J.N., Smutzer, G., Whitty, C.J., Myers, A., Bannon, M.J., 1997. Differential modification of dopamine transporter and tyrosine hydroxylase mRNAs in midbrain of subjects with Parkinson's, Alzheimer's with parkinsonism, and Alzheimer's disease. Mov. Disord. 12, 885–897.
Jürgensen, S., Antonio, L.L., Mussi, G.E.A., Brito-Moreira, J., Bomfim, T.R., De Felice, F. G., Garrido-Sanabria, E.R., Cavalheiro, É.A., Ferreira, S.T., 2011. Activation of D1/D5 dopamine receptors protects neurons from synapse dysfunction induced by amyloid-beta oligomers. J. Biol. Chem. 286, 3270–3276.
Kaczorowski, C.C., Sametsky, E., Shah, S., Vassar, R., Disterhoft, J.F., 2011. Mechanisms underlying basal and learning-related intrinsic excitability in a mouse model of Alzheimer's disease. Neurobiol. Aging 32, 1452–1465.
Kempadoo, K.A., Mosharov, E.V., Choi, S.J., Sulzer, D., Kandel, E.R., 2016. Dopamine release from the locus coeruleus to the dorsal hippocampus promotes spatial learning and memory. Proc. Natl. Acad. Sci. U. S. A. 113, 14835–14840.
Kemppainen, N., Laine, M., Laakso, M.P., Kaasinen, V., Någren, K., Vahlberg, T., Kurki, T., Rinne, J.O., 2003. Hippocampal dopamine D2 receptors correlate with memory functions in Alzheimer's disease. Eur. J. Neurosci. 18, 149–154.
Kheirbek, M.A., Drew, L.J., Burghardt, N.S., Costantini, D.O., Tannenholz, L., Ahmari, S. E., Zeng, H., Fenton, A.A., Hen, R., 2013. Differential control of learning and anxiety along the dorsoventral axis of the dentate gyrus. Neuron 77, 955–968.
Koch, G., Esposito, Z., Codecà, C., Mori, F., Kusayanagi, H., Monteleone, F., Di Lorenzo, F., Bernardi, G., Martorana, A., 2011. Altered dopamine modulation of LTD-like plasticity in Alzheimer's disease patients. Clin. Neurophysiol. 122, 703–707.
Koch, G., Di Lorenzo, F., Bonnì, S., Giacobbe, V., Bozzali, M., Caltagirone, C., Martorana, A., 2014. Dopaminergic modulation of cortical plasticity in Alzheimer's disease patients. Neuropsychopharmacology 39, 2654–2661.
Koch, G., Motta, C., Bonnì, S., Pellicciari, M.C., Picazio, S., Casula, E.P., Maiella, M., Di Lorenzo, F., Ponzo, V., Ferrari, C., et al., 2020. Effect of rotigotine vs placebo on cognitive functions among patients with mild to moderate Alzheimer disease: a randomized clinical trial. JAMA Netw. Open 3, e2010372.
Krashia, P., Cordella, A., Nobili, A., La Barbera, L., Federici, M., Leuti, A., Campanelli, F., Natale, G., Marino, G., Calabrese, V., et al., 2019a. Blunting neuroinflammation with resolvin D1 prevents early pathology in a rat model of Parkinson's disease. Nat. Commun. 10, 3945.
Krashia, P., Nobili, A., D'Amelio, M., 2019b. Unifying hypothesis of dopamine neuron loss in neurodegenerative diseases: focusing on Alzheimer's disease. Front. Mol. Neurosci. 12, 123.
Kumar, U., Patel, S.C., 2007. Immunohistochemical localization of dopamine receptor subtypes (D1R-D5R) in Alzheimer's disease brain. Brain Res. 1131, 187–196.
La Barbera, L., Vedele, F., Nobili, A., Krashia, P., Spoleti, E., Latagliata, E.C., Cutuli, D., Cauzzi, E., Marino, R., Viscomi, M.T., et al., 2021. Nilotinib restores memory function by preventing dopaminergic neuron degeneration in a mouse model of Alzheimer's Disease. Prog. Neurobiol. 202, 102031.
Landfield, P.W., Pitler, T.A., 1984. Prolonged Ca2+−dependent afterhyperpolarizations in hippocampal neurons of aged rats. Science 226, 1089–1092.
LeMasson, G., Marder, E., Abbott, L.F., 1993. Activity-dependent regulation of conductances in model neurons. Science 259, 1915–1917.
Lisman, J.E., Grace, A.A., 2005. The hippocampal-VTA loop: controlling the entry of information into long-term memory. Neuron 46, 703–713.
Marrion, N.V., 1997. Control of M-current. Annu. Rev. Physiol. 59, 483–504.
Martorana, A., Koch, G., 2014. Is dopamine involved in Alzheimer's disease? Front. Aging Neurosci. 6, 252.
Maruszak, A., Thuret, S., 2014. Why looking at the whole hippocampus is not enough-a critical role for anteroposterior axis, subfield and activation analyses to enhance predictive value of hippocampal changes for Alzheimer's disease diagnosis. Front. Cell. Neurosci. 8, 95.
Masters, M.C., Morris, J.C., Roe, C.M., 2015. "Noncognitive" symptoms of early Alzheimer disease: a longitudinal analysis. Neurology 84, 617–622.
McCutcheon, J.E., Conrad, K.L., Carr, S.B., Ford, K.A., McGehee, D.S., Marinelli, M., 2012. Dopamine neurons in the ventral tegmental area fire faster in adolescent rats than in adults. J. Neurophysiol. 108, 1620–1630.
McNamara, C.G., Tejero-Cantero, Á., Trouche, S., Campo-Urriza, N., Dupret, D., 2014. Dopaminergic neurons promote hippocampal reactivation and spatial memory persistence. Nat. Neurosci. 17, 1658–1660.
Migliore, R., Lupascu, C.A., Bologna, L.L., Romani, A., Courcol, J.-D., Antonel, S., Van Geit, W.A.H., Thomson, A.M., Mercer, A., Lange, S., et al., 2018. The physiological variability of channel density in hippocampal CA1 pyramidal cells and interneurons explored using a unified data-driven modeling workflow. PLoS Comput. Biol. 14, e1006423.
Mintun, M.A., Lo, A.C., Duggan Evans, C., Wessels, A.M., Ardayfio, P.A., Andersen, S.W., Shcherbinin, S., Sparks, J., Sims, J.R., Brys, M., et al., 2021. Donanemab in early Alzheimer's disease. N. Engl. J. Med. 384, 1691–1704.
Mondadori, C.R.A., Buchmann, A., Mustovic, H., Schmidt, C.F., Boesiger, P., Nitsch, R. M., Hock, C., Streffer, J., Henke, K., 2006. Enhanced brain activity may precede the diagnosis of Alzheimer's disease by 30 years. Brain 129, 2908–2922.
Monteverde, A., Gnemmi, P., Rossi, F., Monteverde, A., Finali, G.C., 1990. Selegiline in the treatment of mild to moderate Alzheimer-type dementia. Clin. Ther. 12, 315–322.
Moser, M.B., Moser, E.I., 1998. Functional differentiation in the hippocampus. Hippocampus 8, 608–619.
Moyer, J.R., Thompson, L.T., Black, J.P., Disterhoft, J.F., 1992. Nimodipine increases excitability of rabbit CA1 pyramidal neurons in an age- and concentration-dependent manner. J. Neurophysiol. 68, 2100–2109.
Murray, A.M., Weihmueller, F.B., Marshall, J.F., Hurtig, H.I., Gottleib, G.L., Joyce, J.N., 1995. Damage to dopamine systems differs between Parkinson's disease and Alzheimer's disease with parkinsonism. Ann. Neurol. 37, 300–312.
Neuman, K.M., Molina-Campos, E., Musial, T.F., Price, A.L., Oh, K.-J., Wolke, M.L., Buss, E.W., Scheff, S.W., Mufson, E.J., Nicholson, D.A., 2015. Evidence for Alzheimer's disease-linked synapse loss and compensation in mouse and human hippocampal CA1 pyramidal neurons. Brain Struct. Funct. 220, 3143–3165.
Nobili, A., Latagliata, E.C., Viscomi, M.T., Cavallucci, V., Cutuli, D., Giacovazzo, G., Krashia, P., Rizzo, F.R., Marino, R., Federici, M., et al., 2017. Dopamine neuronal loss contributes to memory and reward dysfunction in a model of Alzheimer's disease. Nat. Commun. 8, 14727.
Nobili, A., Krashia, P., Cordella, A., La Barbera, L., Dell'Acqua, M.C., Caruso, A., Pignataro, A., Marino, R., Sciarra, F., Biamonte, F., et al., 2018. Ambra1 shapes hippocampal inhibition/excitation balance: role in neurodevelopmental disorders. Mol. Neurobiol. 55, 7921–7940.
Norrara, B., Fiuza, F.P., Arrais, A.C., Costa, I.M., Santos, J.R., Engelberth, R.C.G.J., Cavalcante, J.S., Guzen, F.P., Cavalcanti, J.R.L.P., Freire, M.A.M., 2018. Pattern of tyrosine hydroxylase expression during aging of mesolimbic pathway of the rat. J. Chem. Neuroanat. 92, 83–91.
Oh, M.M., Simkin, D., Disterhoft, J.F., 2016. Intrinsic hippocampal excitability changes of opposite signs and different origins in CA1 and CA3 pyramidal neurons underlie aging-related cognitive deficits. Front. Syst. Neurosci. 10, 52.
Ordemann, G.J., Apgar, C.J., Brager, D.H., 2019. D-type potassium channels normalize action potential firing between dorsal and ventral CA1 neurons of the mouse hippocampus. J. Neurophysiol. 121, 983–995.
Palop, J.J., Mucke, L., 2016. Network abnormalities and interneuron dysfunction in Alzheimer disease. Nat. Rev. Neurosci. 17, 777–792.
Pazini, A.M., Gomes, G.M., Villarinho, J.G., da Cunha, C., Pinheiro, F., Ferreira, A.P.O., Mello, C.F., Ferreira, J., Rubin, M.A., 2013. Selegiline reverses $a\beta_{25-35}$-induced cognitive deficit in male mice. Neurochem. Res. 38, 2287–2294.
Potier, B., Rascol, O., Jazat, F., Lamour, Y., Dutar, P., 1992. Alterations in the properties of hippocampal pyramidal neurons in the aged rat. Neuroscience 48, 793–806.
Pousinha, P.A., Mouska, X., Bianchi, D., Temido-Ferreira, M., Rajão-Saraiva, J., Gomes, R., Fernandez, S.P., Salgueiro-Pereira, A.R., Gandin, C., Raymond, E.F., et al., 2019. The amyloid precursor protein C-terminal domain alters CA1 neuron firing, modifying hippocampus oscillations and impairing spatial memory encoding. Cell Rep. 29, 317–331.e5.
Rabinovici, G.D., 2021. Controversy and progress in Alzheimer's disease - FDA approval of aducanumab. N. Engl. J. Med. 385, 771–774.
Randall, A.D., Booth, C., Brown, J.T., 2012. Age-related changes to Na+ channel gating contribute to modified intrinsic neuronal excitability. Neurobiol. Aging 33, 2715–2720.
Reiman, E.M., Quiroz, Y.T., Fleisher, A.S., Chen, K., Velez-Pardo, C., Jimenez-Del-Rio, M., Fagan, A.M., Shah, A.R., Alvarez, S., Arbelaez, A., et al., 2012. Brain imaging and fluid biomarker analysis in young adults at genetic risk for autosomal dominant Alzheimer's disease in the presenilin 1 E280A kindred: a case-control study. Lancet Neurol. 11, 1048–1056.
Rinne, J.O., Säkö, E., Paljärvi, L., Mölsä, P.K., Rinne, U.K., 1986a. Brain dopamine D-1 receptors in senile dementia. J. Neurol. Sci. 73, 219–230.
Rinne, J.O., Säkö, E., Paljärvi, L., Mölsä, P.K., Rinne, U.K., 1986b. Brain dopamine D-2 receptors in senile dementia. J. Neural Transm. 65, 51–62.
Rosen, Z.B., Cheung, S., Siegelbaum, S.A., 2015. Midbrain dopamine neurons bidirectionally regulate CA3-CA1 synaptic drive. Nat. Neurosci. 18, 1763–1771.
Rossato, J.I., Bevilaqua, L.R.M., Izquierdo, I., Medina, J.H., Cammarota, M., 2009. Dopamine controls persistence of long-term memory storage. Science 325, 1017–1020.
Rothman, J.S., Silver, R.A., 2018. NeuroMatic: an integrated open-source software toolkit for acquisition, analysis and simulation of electrophysiological data. Front. Neuroinform. 12, 14.
Sala, A., Caminiti, S.P., Presotto, L., Pilotto, A., Liguori, C., Chiaravalloti, A., Garibotto, V., Frisoni, G.B., D'Amelio, M., Paghera, B., et al., 2021. In vivo human molecular neuroimaging of dopaminergic vulnerability along the Alzheimer's disease phases. Alzheimers Res. Ther. 13, 187.
Sara, S.J., 2009. The locus coeruleus and noradrenergic modulation of cognition. Nat. Rev. Neurosci. 10, 211–223.
Sathyanesan, A., Ogura, T., Lin, W., 2012. Automated measurement of nerve fiber density using line intensity scan analysis. J. Neurosci. Methods 206, 165–175.
Serra, L., D'Amelio, M., Di Domenico, C., Dipasquale, O., Marra, C., Mercuri, N.B., Caltagirone, C., Cercignani, M., Bozzali, M., 2018. In vivo mapping of brainstem nuclei functional connectivity disruption in Alzheimer's disease. Neurobiol. Aging 72, 72–82.
Serra, L., D'Amelio, M., Esposito, S., Di Domenico, C., Koch, G., Marra, C., Mercuri, N.B., Caltagirone, C., Artusi, C.A., Lopiano, L., et al., 2021. Ventral tegmental area disconnection contributes two years early to correctly classify patients converted to Alzheimer's disease: implications for treatment. J. Alzheimers Dis. 82, 985–1000.
Storga, D., Vrecko, K., Birkmayer, J.G., Reibnegger, G., 1996. Monoaminergic neurotransmitters, their precursors and metabolites in brains of Alzheimer patients. Neurosci. Lett. 203, 29–32.
Storm, J.F., 1987. Action potential repolarization and a fast after-hyperpolarization in rat hippocampal pyramidal cells. J. Physiol. 385, 733–759.

Storm, J.F., 1990. Potassium currents in hippocampal pyramidal cells. Prog. Brain Res. 83, 161–187.
Strange, B.A., Witter, M.P., Lein, E.S., Moser, E.I., 2014. Functional organization of the hippocampal longitudinal axis. Nat. Rev. Neurosci. 15, 655–669.
Styr, B., Slutsky, I., 2018. Imbalance between firing homeostasis and synaptic plasticity drives early-phase Alzheimer's disease. Nat. Neurosci. 21, 463–473.
Suter, B.A., Migliore, M., Shepherd, G.M.G., 2013. Intrinsic electrophysiology of mouse corticospinal neurons: a class-specific triad of spike-related properties. Cereb. Cortex 23, 1965–1977.
Swanson, C.J., Zhang, Y., Dhadda, S., Wang, J., Kaplow, J., Lai, R.Y.K., Lannfelt, L., Bradley, H., Rabe, M., Koyama, A., et al., 2021. A randomized, double-blind, phase 2b proof-of-concept clinical trial in early Alzheimer's disease with lecanemab, an anti-Aβ protofibril antibody. Alzheimers Res. Ther. 13, 80.
Taglialatela, G., Hogan, D., Zhang, W.-R., Dineley, K.T., 2009. Intermediate- and long-term recognition memory deficits in Tg2576 mice are reversed with acute calcineurin inhibition. Behav. Brain Res. 200, 95–99.
Ting, J.T., Lee, B.R., Chong, P., Soler-Llavina, G., Cobbs, C., Koch, C., Zeng, H., Lein, E., 2018. Preparation of acute brain slices using an optimized N-Methyl-D-glucamine protective recovery method. J. Vis. Exp. 132, 53825.
Trombin, F., Gnatkovsky, V., de Curtis, M., 2011. Changes in action potential features during focal seizure discharges in the entorhinal cortex of the in vitro isolated guinea pig brain. J. Neurophysiol. 106, 1411–1423.
Tsunekawa, H., Noda, Y., Mouri, A., Yoneda, F., Nabeshima, T., 2008. Synergistic effects of selegiline and donepezil on cognitive impairment induced by amyloid beta (25-35). Behav. Brain Res. 190, 224–232.
Turrigiano, G., 2011. Too many cooks? Intrinsic and synaptic homeostatic mechanisms in cortical circuit refinement. Annu. Rev. Neurosci. 34, 89–103.
Turrigiano, G.G., Leslie, K.R., Desai, N.S., Rutherford, L.C., Nelson, S.B., 1998. Activity-dependent scaling of quantal amplitude in neocortical neurons. Nature 391, 892–896.
Venneri, A., De Marco, M., 2020. Reduced monoaminergic nuclei MRI signal detectable in pre-symptomatic older adults with future memory decline. Sci. Rep. 10, 18707.
Xu, F., Ono, M., Ito, T., Uchiumi, O., Wang, F., Zhang, Y., Sun, P., Zhang, Q., Yamaki, S., Yamamoto, R., et al., 2021. Remodeling of projections from ventral hippocampus to prefrontal cortex in Alzheimer's mice. J. Comp. Neurol. 529, 1486–1498.
Yang, K., Broussard, J.I., Levine, A.T., Jenson, D., Arenkiel, B.R., Dani, J.A., 2017. Dopamine receptor activity participates in hippocampal synaptic plasticity associated with novel object recognition. Eur. J. Neurosci. 45, 138–146.
Zarei, M., Beckmann, C.F., Binnewijzend, M.A.A., Schoonheim, M.M., Oghabian, M.A., Sanz-Arigita, E.J., Scheltens, P., Matthews, P.M., Barkhof, F., 2013. Functional segmentation of the hippocampus in the healthy human brain and in Alzheimer's disease. Neuroimage 66, 28–35.